INSTITUTE FOR DIRECT ENERGY CONVERSION

TOWNE SCHOOL

UNIVERSITY OF PENNSYLVANIA

PHILADELPHIA, PENNSYLVANIA

STATUS REPORT

INDEC-SR-12

NATIONAL AERONAUTICS AND SPACE ADMINISTRATION

GRANT NSG-316

JUNE 1967

INSTITUTE FOR DIRECT ENERGY CONVERSION

TOWNE SCHOOL

UNIVERSITY OF PENNSYLVANIA

PHILADELPHIA, PENNSYLVANIA

MANFRED ALTMAN, DIRECTOR

STATUS REPORT

INDEC-SR-12

NATIONAL AERONAUTICS AND SPACE ADMINISTRATION

GRANT NSG - 316

June 1967

TABLE OF CONTENTS

1. MATERIALS ENGINEERING

Branch Chief: Dr. Solomon Pollack

Senior Members: Dr. Manfred Altman, Dr. Louis Girifalco,

1.1 High Temperature Thermal Diffusivity Measurement

Senior Investigator: Dr. Manfred Altman

Ph. D. Student: K. Sreenivasan

Objectives

To develop an experimental technique suitable for the determination of thermal diffusivity at high temperature, primarily for the testing of thermal energy storage materials in the liquid state.

Previous Accomplishments

Phase 1: The theory of transient technique was studied and a new technique applicable to liquids was developed.

Phase 2: The furnace and the measuring equipment were designed and built.

Phase 3: The thermal diffusivity of the container material - boron nitride - was measured.

Phase 4: The thermal diffusivity of liquid lithium fluoride was measured.

Phase 5: The method and the cell were calibrated by measuring the diffusivity of liquid sodium nitrate.

Progress in Past Period

The thermal diffusivity of lithium fluoride in the solid and the liquid states were compared and empirical correlation for the thermal conductivity at the melting point was developed. A doctoral dissertation based on this work is under preparation. Details are presented on page A1-1 through A1-7.

1.1 High Temperature Thermal Diffusivity Measurement

Senior Investigator: Dr. Manfred Altman

Graduate Student: H. Keramaty

Objectives

To develop experimental techniques suitable for the measurement of thermal diffusivity of solid mixtures, primarily for the determination of the diffusivity of materials which do not lend themselves to large physical samples to be measured directly.

Previous Accomplishments

A vacuum furnace capable of 2300^{o}C was designed, built, and checked. Diffusivity of solid lithium fluoride was measured.

Thermal diffusivity of CaF_2, BaF_2, and two of their mixtures was measured.

Progress in Past Period

Thermal diffusivities of MgF_2, CaF_2, and a mixture of the two was measured.

1.2 Experimental Determination of the Thermoelectric Properties of Graphite Alloys

Senior Investigator: Dr. S. R. Pollack

Graduate Student: J. J. Curry

Objectives

Since graphite-compounds are not available for study, it was decided that certain semiconductors belonging to the I - II_2 - III - VI_4 class should be investigated. One compound $CuCd_2$ In Te_4 was selected because it has a fairly high thermoelectric power. The compound will be studied to determine

1) thermoelectric power
2) electrical resistivity
3) carrier concentration
4) thermoelectric figure of merit

Previous Accomplishments

(1) Construction of necessary equipment to measure resistivity, thermoelectric power and carrier concentration as a function of temperature.

(2) Development of a method to produce samples of reproducible properties and flexibility of sample geometry, the latter involving powder-metallurgical techniques.

Progress in Past Period

The following information has been obtained over the range of 100°K to 300°K

(1) thermoelectric power

(2) electrical resistivity

(3) carrier concentration

(4) carrier mobility

Work is nearing completion on the apparatus to measure the figure of merit between 300°K and 600°K.

Investigation is now under way to determine the effects of stoichiometric differences on the thermoelectric properties of the compound by studying the system $CuCd_{2-x}In_{1+x}Te_4$. Details on page A1-11 through A1-14.

1.3 Tunnel Emission Cold Cathodes

Senior Investigator: Dr. S. R. Pollack

Graduate Student: S. Basavaiah

Objectives

The principle objective is to investigate the structure of metal-oxide-metal thin film junctions using refractory metal oxide systems. The transport phenomena of electrons through thin oxide films will be studied.

Previous Accomplishments

Vacuum system with 5×10^{-9} torr. ultimate pressure and accessories for the fabrication of tunnel junctions were assembled. Equipment to take I-V-T data over a current range of 10^{-9} amperes to 10^{-1} amperes and over a temperature range of 77°K to 300°K was put into operation. Some tungsten-tungsten oxide-gold junctions were made and their characteristics were studied at room temperature.

Progress in Past Period

A number of tungsten-tungsten oxide-gold junctions were prepared with varying oxide thickness. I-V-T data on the samples are being taken. The initial data has led to the following conclusions. The current is an exponential function of voltage and approximately can be represented by $I = A \exp(BV^{1/2})$ at a particular temperature, over 3 to 4 decades of current range. The functional dependence of current upon temperature is being studied.

At this point, it can be said that the temperature dependence is too large to be explained by tunneling theory between 110°K and 300°K. Unfortunately, the effects of temperature can not be explained by Schottky emission either. Details on page A1-15 through A1-20.

1.4 Studies of Thermal Transpiration for the Development of a "Thermal Pump"

Senior Investigator: Dr. Manfred Altman

Graduate Student: Mr. E. Hopfinger

Objectives

To develop a gas pump without moving parts based on the thermal transpiration principle.

Previous Accomplishments

Theoretical analysis of idealized system and preliminary experiments which showed the general characteristics of such a pump.

Progress in Past Period

Theoretical analysis of real systems and partial evaluation of experimental data. Details on page A1-21 through A1-30.

2.1 Slow Wave Plasma Diagnostics

W. H. Becker L. W. Zelby

Objectives

To develop slow wave plasma interaction for measurement of local plasma parameters.

Progress in Past Period

The plasma helix system was reinvestigated because of some discrepancy between the measured and calculated values (see INDEC SR-9). The modified results are shown in Figures 1-6 on pages A2-13 through A2-18. Some additional modes can be noted in the fast wave region (see Figure 1). It will also be noted that the large argument for representation yields an adequate dispersion relation for the system in question.

2. PLASMA ENGINEERING

Branch Chief: Leon W. Zelby

Senior Members: Michael Kaplit, George Schrenk, Samuel Schweitzer, Hsuan Yeh

2.2 Experimental Study of an Electromagnetically Driven Mercury Centrifuge

S. Schweitzer I. M. Cohen*

T. Ebtekar

Objectives

To study the operation parameters of a mercury centrifuge.

Previous Accomplishments

Design of a simple mercury centrifuge, driven electromagnetically has been completed. Provisions for measurements of velocity and pressure distributions have been made. Apparatus has been constructed.

Progress in Past Period

We have made measurements of the following parameters of the magnet in the absence of the device:

(1) Time dependence of z component of magnetic field

(2) B_z as a function of r at various z = constant planes.

*Associate Professor of Mechanical Engineering, Towne School of Civil and Mechanical Engineering, University of Pennsylvania

The variation of V_{θ} as a function of r while the device is in operation has been measured by total and static pressure tubes.

The variation of B_{θ} as a function of z has been measured in the mercury filled device in the absence of an applied magnetic field.

The results are given in Figures 1-4 of the Appendix, page A2-1 through A2-4.

2.3 The Flow of a Conducting Liquid in an Annular Gap

S. Schweitzer I. M. Cohen*

Objectives

To study the flow field, current distribution, and magnetic field in an annular gap filled with a conducting fluid and driven electromagnetically.

Previous Accomplishments

One-dimensional, inviscid flow of mercury in an annular gap, driven electromagnetically has been studied. A restricted nonexistence proof was given (see progress rep. SR-11).

Progress in Past Period

Complete nonexistence of solutions to the problem as formulated in progress report SR-11 has been proved. We are now concentrating on the effects of secondary flow created by the body force.

*Associate Professor of Mechanical Engineering, Towne School of Civil and Mechanical Engineering, University of Pennsylvania.

2.4 First Order Effects of Production on the Continuum Theory of Spherical Electrostatic Probes[†]

I. M. Cohen* S. Schweitzer

Objectives

To study the first order effects of ionization and recombination on the continuum theory of spherical electrostatic probes.

Previous Accomplishments

None.

Progress in Past Period

The analysis of spherical Langmuir probes which are immersed in an infinite, homogeneous, slightly ionized, collision-dominated plasma is given to first order in the smallness of a parameter characterizing the effects of ionization and recombination. The treatment is given as a double limit: mean free path $<<$ sheath thickness $<<$ probe radius (as in the antecedent

*Associate Professor of Mechanical Engineering, Towne School of Civil and Mechanical Engineering, University of Pennsylvania.

[†]Submitted for publication to the AIAA Journal. To be presented at the AIAA Joint Electric Propulsion and Plasmadynamics Conference, Colorado Springs, Sept. 11-13, 1967.

works) and the weakness of production effects. The first limit separates the system of equations into two regions: a quasi-neutral region and a thin collision-dominated space charge sheath. The second limit of weak production further separates the quasi-neutral region into two subsidiary regions: a main region in which the production effect is a regular perturbation and a distant region where gradients are weak and the small production is of the same order as diffusion. The governing diffusion equations are solved to lowest order in $\rho_p = r_p/\lambda_D$ and to first order in the smallness of the production parameter. Current-voltage characteristics are computed from integrals of the solutions and emphasis is placed on their interpretation with respect to measurements. An experimental procedure is outlined which yields in turn $D_- N_o$, T_-/T_+, D_+/D_-, and the production parameter, where D is diffusion coefficient, T is temperature and N_o is the undisturbed ion or electron density. The first order effects of ionization and recombination are also discussed. It is found for $T_-/T_+ = 1$ that, at negative probe potentials, the normalized ion current to the probe is increased and the electron current decreased. At positive probe potentials, on the other hand, the ion current to the probe is decreased and the electron current increased by the effect of production. For $T_-/T_+ > 1$, the same effect is observed for negative probe potentials but, for positive probe potentials, no such general statement can be made. For a ten percent change in the production parameter, for example, we find that the relative change in the currents is at most slightly more than ten percent (for fixed probe potential).

(For more details, see INDEC Report 47; a paper based on this report is to be published in the A.I.A.A. Journal.)

2.5 The Influence of High Fields on Surface Charge Distributions

G. L. Schrenk S. Fonash

Objectives

To determine the effect of high fields on the work function of metals.

Previous Accomplishments

Research is in progress to understand the varying average intensity of the different regions of field ion micrographs. These regions are rather sharply defined and are more pronounced in some metals than in others - e.g., in platinum they form one of the most prominent features of the micrograph, while in tungsten they are barely discernible.

One possible explanation of these sharply defined regions is that they are related to the band structure of metals at their Fermi levels. We only need to consider the Fermi level because tunneling occurs only to the Fermi level of the metal at the low temperature and high field strengths involved.

Progress in Past Period

Current research is focused on the construction of a quantum mechanical model of this tunneling process. Because of the lack of knowledge of the Fermi surfaces of the metals involved, considerable research is also being devoted to investigating the Fermi surfaces involved. The detailed mathematical model has been constructed; current efforts are being devoted to the numerical evaluation of the various segments of the model. Results will be made available in future reports.

2.6 Electrical Conductivity of Partially Ionized Gases

S. Schweitzer

Objectives

Evaluation of mixture rules to calculate the tensor electrical conductivity of ionized gases.

Previous Accomplishments

Evaluations of present mixture rules for the calculation of the tensor electrical conductivity of partially ionized gases have been made. A new mixture rule for the tensor conductivity has been proposed and evaluated. All evaluations are based on the third Chapman-Enskog approximation.

For details see INDEC reports 20, 31, 35, 39.

Progress in Past Period

The accuracy of Frost's mixture rule for the scalar electrical conductivity at very low levels of ionization has been examined. It is shown that at low degrees of ionization Frost's results may overestimate the electrical conductivity. Details are to be published in the J. AIAA. See Appendix pages A2-5 through A2-12.

2.7 Characteristics of Thermionic Plasma Diodes with Gas Mixtures

G. L. Schrenk A. Kaufman

Objectives

To investigate the engineering significance of cesium thermionic converters seeded with gases exhibiting the Penning effect. In particular, this research seeks to determine if the addition of mercury or cadmium to a cesium thermionic diode will increase the maximum output power of the diode.

Summary

The purpose of this research was to investigate whether adding mercury or cadmium to a cesium diode would result in an increase in the maximum output power of a wide-spaced diode. The main emphasis was on the ignited mode since the maximum output power of a wide-spaced diode occurs in the ignited mode.

The initial step in this research was the development of a phenomenological macroscopic model for the ignited mode. The model was developed using the principles of conservation of mass, charge, current, and energy at the plasma edges. A similar model was also developed for the unignited mode.

The relationship between the electron density and the electron temperature in the plasma of the diode was calculated by the use of rate equations and a nine-level atomic model for cesium. It was found that the higher the pressure or electron temperature of the plasma, the greater the agreement between the results of the present model and the Saha equation. The results deviate from the Saha equation at low pressure or at low electron temperature because radiative effects in the plasma become important.

In the case of a pure cesium diode, the electron temperature predicted by the model used in this research agrees rather well with known experimental values. Most of the previous models for the ignited mode predict temperatures about 500°K higher than the known experimental values.

The introduction of mercury or cadmium into the cesium diode results in a Penning effect in the plasma. In this research, it was shown that the addition of mercury resulted in no significant change in the electron density of the plasma because the excitation energy of mercury is about 1 eV higher than the ionization energy of cesium. The excitation energy of cadmium is at the same level as the ionization energy of cesium; thus, the addition of cadmium can result in a large change in the electron density of the diode. For diodes with cesium densities in the range of 5×10^{19} atoms/m^3 to 5×10^{24} atoms/m^3, adding cadmium to a cesium diode at a ratio of one hundred to one results in gains as high as sixty in electron density at a given electron temperature.

The output voltage-current curves for both the unignited and ignited modes were calculated in this research. It was shown that the addition of cadmium to the cesium diode results in the diode operating at a higher electron density and at a lower electron temperature. It was found that when the cesium diode is seeded with a cadmium to cesium ratio of one hundred to one, the output current can increase by as much as a factor of four. It was also shown that in many cases the increase in the output current is proportional to the increase in the electron density. It was also found that seeding the diode with cadmium could remove the unignited mode at a lower cesium pressure. This could be important if it is desirable to eliminate the unignited mode and to use as low a cesium pressure as possible (because of material problems, etc.). The removal of the unignited mode can result in an improvement in the stability of the system.

The addition of mercury results in a decrease in the output current of the diode in the unignited mode. This decrease is caused by the fact that the addition of mercury results in a large increase in the collision cross section of the diode but in a negligible increase in the electron density of the diode.

The addition of cadmium to the cesium diode results in the diode operating at a lower electron temperature and at a higher electron density. It was found that in the ignited mode the gain in the electron density is much smaller than the gain in the total collision cross section. The fact that the increase in the total collision cross section is larger than the increase in the electron density results in a small increase in the output voltage (no more than five per cent) and in some cases in a decrease. It was shown that the increase in the output current is at least an order of magnitude lower than the increase in the electron density. Thus, unlike the unignited mode, seeding will not result in any significant increase in the output current in the ignited mode. Since the addition of cadmium results in very little gain in the output current and voltage, the gain in the maximum power is very small. It was found that the addition of cadmium to a cesium diode in the ignited mode results in the maximum output power increasing by, at most, six per cent. In some cases, the addition of cadmium results in a decrease in the output power of the diode. The addition of mercury results in no enhancement in the ignited mode.

In conclusion, it can be said that adding mercury to a cesium diode does not result in any significant improvement in the performance of the diode. The addition of cadmium results in some enhancement in the performance of the diode in the unignited mode. In the ignited mode, the addition of cadmium does not result in any significant enhancement in the

maximum output power of the diode. Thus, it must be concluded that the engineering significance of a mercury-cesium or cadmium-cesium diode is minimal.

Progress in Past Period

This research project has been completed and is the basis of Allen Kaufman's Ph. D. dissertation.

3. ELECTROCHEMICAL ENGINEERING

Branch Chief: Dr. Leonard Nanis

Senior Member: Dr. John O' M. Bockris

Postdoctoral Research Associate: Dr. Philippe Javet

3.1 Freezing Potentials

Senior Investigator: Dr. L. Nanis

Graduate Student: Irving Klein

OBJECTIVES

The present research serves to investigate the effect of the experimental parameters in general and the freezing substrate in particular on the interface potential developed when a dilute ionic solution is frozen.

PREVIOUS ACCOMPLISHMENTS

It has been shown that the following experimental parameters affect the "freezing potential": 1) the type of ionic species dissolved in the solution; 2) the concentration of the dissolved ions; 3) the type of substrate upon which freezing takes place. In trying to investigate which properties inherent to the freezing substrate affect the potential, it has been shown that the potential of zero charge is of negligible importance, and that the thermal diffusivity is of moderate importance. It became apparent, however, that some other property of the substrate plays a significant role.

PROGRESS IN PAST PERIOD

It has been conclusively proven that the chemical composition of the substrate's surface has a very large effect on the "freezing potential." Specifically, the presence of a thin oxide film on a mercury surface can completely negate any "freezing potential." A master's thesis was written culminating the efforts of the last year of research. The remainder of this report will therefore summarize the pertinent aspects of this thesis.

See page A3-1 through A3-5 for details.

3.2 Current and Potential Distribution in Cylindrical Geometries: Engineering Application to Fuel Cell Design

Senior Investigator: Dr. L. Nanis

Graduate Student: Wallace Kesselman

OBJECTIVES

The purpose of these efforts is to develop simplified treatments of the mathematics which underlie fuel cell design and behavior. For engineering purposes, the compact notation favored by mathematicians is elegant but not useful. Attention will be devoted to simplifying the mathematics wherever possible and indicating design parameters which evolve in consideration of potential and current distribution in porous electrode models and related heat and mass transfer computations.

PREVIOUS ACCOMPLISHMENTS

Potential and current distributions have been represented analytically as a function of position near a conducting disk for two cases; namely, primary current distribution and uniform current distribution.

PROGRESS IN PAST PERIOD

The intermediate case of a current distribution lying between primary and uniform has been investigated. The problem has been reduced to solving a singular linear Fredholm integral equation of the second kind. Details on pages A3-6 through A3-8.

3.3 Foaming Electrolyte Fuel Cell

Senior Investigator: Dr. L. Nanis
Research Specialist: A. P. Saunders

OBJECTIVES

This work derives from considerations of diffusion as an ultimate fuel cell limitation step and methods to avoid the use of porous electrodes. Rapid gas saturation into electrolyte can be accomplished by providing large contact area and short diffusion path. Electrolyte foam is theoretically ideal for this purpose and laboratory studies are needed to verify this approach.

PREVIOUS ACCOMPLISHMENTS

A surfactant needed to produce a stable foam in KOH electrolyte was found. Initial experiments confirmed that a platinum electrode immersed in foam could support a higher reaction rate than a platinum electrode immersed in non-foaming KOH electrolyte with the fuel gas bubbling through it at a high flow rate.

PROGRESS IN PAST PERIOD

A series of experiments have been initiated to obtain qualitative comparisons of mass transport characteristics between Pt electrodes immersed in a fuel saturated, stirred electrolyte, and an electrode immersed in a foam structured electrolyte. A previously unreported cyclic alternation of anode potential has been found with evidence for a complex controlling current.

3.4 Atomic Scale Electrode Processes

P. Javet L. Nanis

Objectives

Application of the newly developed method of Field Ion Microscopy to the study of electrode surfaces. Ultimately, the method should provide a visualization of atomic processes occurring at the surface of a metal as a result of electrochemical treatment. As a first study, we have examined the behavior of gases on noble metal electrodes, particularly as a result of anodic treatment.

Previous Accomplishments

The operation of a commercial model F.I.M. (Central Scientific Company) was checked with W tips (giving good resolution) and Pt (fair resolution).

Progress in Past Period

Systematic investigation of best conditions of image formation have shown that Pt is not suitable for use in our case. Iridium tips have been successfully prepared and imaged with satisfactory resolution. For details, see page A3-15.

3.5 Galvanostatic Transients

L. Nanis P. Javet

Objectives

To develop a simple and practical mathematical treatment for the time variation of activation overpotential following switching on or off of a constant current, particularly in the cases where the double layer capacity is not constant.

Previous Accomplishments

Useful mathematical relations have been developed for charging transients. A potential dependent capacity may be introduced in the formula (published J. Electrochem. Soc. 114, 810 (1967)).

Progress in Past Period

The above mentioned treatment has been extended to discharging transients. A non-constant, potential dependent capacity changes the time variation of activation overpotential up to 30%. For details, see page A3-17.

4. PUBLICATIONS LIST

Publications List

INDEC-1 "The Optimization of MHD Generators with Arbitrary Conductivity", H. Yeh and T. K. Chu, ASME Paper 63-WA-349.

INDEC-2 "The Prediction of Transient Heat Transfer Performance of Thermal Energy Storage Devices", M. Altman, D. P. Ross, H. Chang, Proceedings of 6th National Heat Transfer Conference, Boston, Mass., 1963.

INDEC-3 "The Binary Eutectic as a Thermal Energy Storage System: Equilibrium Properties", G. R. Belton and Y. K. Rao, paper presented at the 6th National Heat Transfer Conference Boston, Mass., Aug. 11-14, 1963.

INDEC-4 "Theoretical Model of a Thermionic Converter", J. Dunlop and G. Schrenk, Proceedings of Thermionic Specialist Conference, Gatlinburg, Tenn., pp. 57-62, Oct. 7-9, 1963.

INDEC-5 "Thermophysical and Transport Properties of High Temperature Energy Storage Materials", R. Sharma and H. Chang, paper presented at the Third Annual Symposium, High Temperature Conversion Heat to Electricity, Tucson, Arizona, Feb. 19-21, 1964.

INDEC-6 "Solar Collection Limitations for Dynamic Converters - Simulation of Solar-Thermal Energy Conversion Systems", G. L. Schrenk, Proceedings of AGARD Conference, Cannes, France, March 16-20, 1964.

INDEC-7 "Prospects for Thermal Energy Storage", M. Altman, Proceedings of AGARD Conference, Cannes, France, March 16-20, 1964.

INDEC-8 "The Hollow Thermionic Converter", L. Zelby, IEEE Annual Meeting on Energy Conversion, Clearwater, Florida, May, 1964.

INDEC-9 "The Institute for Direct Energy Conversion", M. Altman, paper presented at Am. Soc. Eng. Ed. Annual Meeting, University of Maine, Orono, Maine, June 22-26, 1964.

INDEC-10 "Emitter Sheath Polarity in Plasma Diodes", G. Schrenk, Proceedings of Thermionic Specialist Conference, Cleveland, Ohio, Oct. 26-28, 1964, pp. 249-257.

INDEC-11 "Electron Emission from Metals in Gaseous Environment", M. Kaplit, G. Schrenk, L. Zelby, Proceedings of Thermionic Specialist Conference, Cleveland, Ohio, Oct. 26-28, 1964, pp. 4-10.

INDEC-12 "Criteria for Emitter Sheath Polarity in Plasma Diodes", G. Schrenk, paper presented at ASME Winter Annual Meeting New York, No. 29, Dec. 3, 1964.

INDEC-13 "An Electrochemical and Microbiological Study of the Formic Acid-Formic Dehydrogenlyase System", R. J. Blasco and E. Gileadi, Advanced Energy Conversion, Vol. 4, pp. 179-186, 1964.

INDEC-14 "Mathematical Simulation of Solar Thermionic Energy Conversion Systems", G. Schrenk and A. Lowi, Proceedings of the International Thermionic Electrical Power Generation Conference, IEEE, London, England, Sept. 20-24, 1965.

INDEC-15 "Cavity Receiver Temperature Analysis", R. McKinnon, A. Turrin, G. Schrenk, AIAA paper No. 65-470, July 26-29, 1965.

INDEC-16 "Electron Emission from Metals in Vapors of Cesium and Fluorine", G. Schrenk and M. Kaplit. Proceedings of the Thermionic Specialist Conference, San Diego, California, Oct. 25-27, 1965.

INDEC-17 "Longitudinal Interaction of Microwaves with an Argon Discharge", C. A. Renton and L. W. Zelby, Appl. Phys. Ltrs., Vol. 6, No. 8, pp. 167-169, September 15, 1965.

INDEC-18 "Microwave Interaction with a Non-Uniform Argon Discharge", L. W. Zelby, Proceedings of the Symposium of Microwave Interaction with Ferrimagnetics and Plasmas, London, England, pp. 32-1 to 32-3, Sept. 13-17, 1965.

INDEC-19 "Two-Phase Flow and Heat Transfer for Boiling Liquid Nitrogen in Horizontal Tubes", M. Altman and J. H. Jones, Chemical Engineering Progress Symposium Series, Volume 61, No. 57, Oct. 1965.

INDEC-20 "Electrical Conductivity of a Partially Ionized Gas in a Magnetic Field", S. Schweitzer and M. Mitchner. Physics of Fluids, 10, 799-806 (1967).

INDEC-21 "Models for Electron Emission from Metals with Adsorbed Monolayers", M. Kaplit, G. L. Schrenk, and L. Zelby. Advanced Energy Conversion, in press.

INDEC-22 "Models for Electron Emission from Metals with Adsorbed Monolayers", M. Kaplit and G. L. Schrenk. Proceedings of the Twenty-Sixth Annual Conference on Physical Electronics, Massachusetts Institute of Technology, Cambridge, Mass., March 21-23, 1966.

INDEC-23 "Slow Wave Interaction with an Argon Discharge", (Abstract) L. W. Zelby, Symposium on Properties and Applications of Low-Temperature Plasmas, XX-th International Congress of I.V.P.A.C., Moscow, USSR, July 15-18, 1965.

INDEC-24 "Understanding Plasma Diodes and Amplifiers", L. W. Zelby, Electronic Industries, Vol. 24, No. 11, p. 64, Nov. 1965.

INDEC-25 "A Simplified Approach to the Analysis of Electromagnetic Wave Propagation Characteristics of Plasma Coated Surfaces", L. W. Zelby, RCA Review, Vol. 26, No. 4, p. 497, Dec. 1965.

INDEC-26 "Plasma Coated Surface as aWave Guide", L. W. Zelby, RCA Engineer, Vol. 11, No. 4, p. 50, Jan. 19, 1966.

INDEC-27 "Measurements of Collision Frequency in an Argon Discharge", L. W. Zelby, W. O. Mehuron, R. Kalagher, Applied Physics Letters, June 15, 1966, Vol. 21, No. 5, pp. 522-524.

INDEC-28 "Effects of Inhomogeneous Electron Density in a Cylindrical Plasma Column Surrounded by a Helix", R. Kalagher, Submitted to IEEE Transactions on Microwave Theory and Techniques, March 1966.

INDEC-29 "Syringe for Injecting Sodium Potassium Alloy", Samuel Greenhalgh, The Review of Scientific Instruments, Vol. 38, No. 1, pp. 121-122, January 1967.

INDEC-30 "Characteristics of Plasma Probes in a MHD Working Fluid", A. Whitman, H. Yeh, presented at International Symposium on Magnetohydrodynamic Electrical Power Generation, Salzburg, Austria, July 4-8, 1966.

INDEC-31 "Convergence of Successive Approximations to the Scalar Electrical Conductivity of Some Weakly Ionized Real Gases", S. Schweitzer, M. Mitchner, published in the A.I.A.A. Journal, Volume 5, No. 2, pp. 351-353, 1967.

INDEC-32 "The Determination of Thermal Diffusivities of Thermal Energy Storage Materials, Part 1, Solids Up To Melting Point", Han Chang, Manfred Altman, Ram Sharma. Accepted for publication in the A.S.M.E. Journal.

INDEC-33 "Electrochemical Principles of Corrosion", Leonard Nanis, presented at the National Association of Corrosion Engineers Symposium, September, 1966, Philadelphia, Penna.

INDEC-34 "Tolerance Specification by Multiple Alignment Statistics", L. Nanis, presented at Session 14 "Effective Utilization of Grid-Based Interconnection Systems", proceedings of the 1966 Western Electronic Show and Convention, Los Angeles, California, August, I.E.E.E.

INDEC-35 "The Tensor Electrical Conductivity of Atmospheric Cesium-Seeded Argon", S. Schweitzer, A.I.A.A. Journal, Volume 5, No. 5, pp. 844-846 (1967).

INDEC-36 "The Reaction of Molten Metal Droplets with a Rarefield Atmosphere", by M. Altman, D. Ross. Published in the A.I.A.A. Journal, April 1967, Vol. 5, No. 4.

INDEC-37 "Electron Transfer Processes Through Tantalum-Tantalum Oxide Diodes", S. Pollack. Journal of Applied Physics, November, 1966.

INDEC-38 "A Method for Determination of the Permeation Rate of Hydrogen Through Metal Membranes", J. McBreen, W. Beck, L. Nanis, Journal of Electrochemical Society, 113, No. 11, pp. 1218-1222 (November 1966).

INDEC-39 "Tensor Electrical Conductivity of a Partially Ionized Gas in a Magnetic Field", S. Schweitzer and M. Mitchner. Physics of Fluids, 10, 799-806 (1967).

INDEC-40 "New Method of Producing Electric Power by Means of a Thermionic Converter". Patent application by M. Altman.

INDEC-41 "A Metal-Oxide Thin Film Photovoltaic Energy Converter". Patent application by M. Altman and S. R. Pollack.

INDEC-42 "Current & Potential Distribution in Cylindrical Geometries: Engineering Applications", L. Nanis, submitted to Journal Electrochemical Society, to be presented at Current Distribution Symposium, Dallas, May 1967 Meeting, Electrochemical Society.

INDEC-43 "Overpotential-Time Variation for Galvanostatic Charging with Potential Dependent Capacitance", L. Nanis, P. Javet, Accepted for publication in the Journal of The Electrochemical Society, August 1967 issue.

INDEC-44 "Galvanostatic Charging with Potential Dependent Double Layer Capacitance", L. Nanis, P. Javet, to be submitted to Electrochimica Acta.

INDEC-45 "Decay of Overpotential from the Tafel Region with Potential Dependent Double Layer Capacitance", L. Nanis, P. Javet, to be submitted to Journal of Electrochemical Society.

INDEC-46 "Status of Magnetohydrodynamic Power Generation for Terrestrial Applications", H. Yeh, presented at the A.I.A.A. Third Annual Meeting in Boston, Massachusetts, Nov. 29 - Dec. 2, 1966.

INDEC-47 "First Order Effects of Production on the Continuum Theory of Spherical Electrostatic Probes", Ira M. Cohen and S. Schweitzer, February, 1967.

INDEC-48 "The Electric Automobile - A Discussion of Strategy, Tactics, and Leadership", M. Altman, presented at the National Electric Automobile Symposium, San Jose, California, February 24, 25, 1967.

INDEC-49 "The Electric Automobile - Its Future", M. Altman, presented at the IEEE International Convention, New York, March 20 - 23, 1967.

INDEC-50 "A Method of Accelerating the MRD Method When Sharp Ridges are Present", F. A. Costello and G. L. Schrenk. Submitted to J. Comp. Physics.

INDEC-51 "Numerical Solution to the Heat Transfer Equation with Combined Conduction & Radiation", F. A. Costello and G. L. Schrenk. J. Comp. Physics, Vol. I (1967).

INDEC-52 "The Optimization of Space-Craft Coating Patterns for Temperature Control", F. A. Costello, T. P. Harper, R. Kidwell, and G. L. Schrenk. A.S.M.E. -A.I.Ch.E. Conference, August 6-9, 1967. Paper 67-HT55.

INDEC-53 "Flow of a Conducting Liquid in an Annular Gap: A Restricted Nonexistence Proof", I. M. Cohen and S. Schweitzer. A.I.A.A. Journal, Vol. 5, No. 11, pp. 2066-2068.

INDEC-54 "The Determination of Thermal Diffusivities of Thermal Energy Storage Materials, Part II: Molten Salts Beyond the Melting Point", K. Sreenivasan, M. Altman. To be published in ASME (Journal of Power).

INDEC-55 "Temperature Measurement of an Alkali Metal-Seeded Plasma in an Electric Field", T. K. Chu and Chad F. Gottschlich. To be published in the A.I.A.A. Journal.

INDEC-56 "On the Accuracy of Calculating the Scalar Electrical Conductivity at Very Low Ionization Levels", S. Schweitzer. Published in the A.I.A.A. Journal, Vol. 5, No. 11, pp. 2086-2087.

MATERIALS ENGINEERING

APPENDIX

A-1

Thermal Diffusivity of Liquids

Senior Investigator: Dr. Manfred Altman
Ph.D. Student: K. Sreenivasan

The theory and the experimental details of the method have been described in previous reports. Fundamentally, the difference between the temperature at the surface and at the center of a cylindrical container is measured for a constant rate of surface temperature rise. The liquid, whose thermal diffusivity is to be measured, is contained in an annular groove concentric with the surface. Note that it is not necessary to measure the temperature of the liquid. The width of the groove is so small as to maintain "creeping thermal motion" in the liquid. This minimizes free convection effects to a negligible value.

The thermal diffusivity of the container material is essential for calculating liquid thermal diffusivity. This report presents the experimental results for the thermal diffusivity of the container material. The experimental technique is similar to the one described above with this difference--the cylindrical container is replaced by a solid cylindrical specimen. The material of the specimen is boron nitride. The surface temperature and the difference between the surface temperature and the temperature at the center are monitored in separate recorders. The thermal diffusivity of the specimen is calculated using the recorder data. The experimental results are presented in Fig. 1.

A new 2 3/8" Dia. Pt -40% Rh wire-wound-furnace has been designed and built. This was used for the liquid diffusivity measurements. The results are presented in the next section.

Experimental Results

It was decided to calibrate liquid-diffusivity cell by testing a liquid whose thermal diffusivity has been measured by other investigators. Sodium nitrate (melting point 306.8^{o}C) was chosen as the liquid. Sodium nitrate was tested in the 0.0625 inch annular gap container. The results are shown in Fig. 2. As seen in this figure, the results of this investigation compare very favourably with the results of Bloom et al (Ref. 1).

Lithium fluoride liquid was tested in two containers whose gap widths were different, in order to detect the influence of free convection. It may be recalled that the influence of free convection is proportional to the cube of the gap width. The results obtained with both the containers are shown in Fig. 3. No discernible difference exists in these results. It is reasonable to conclude that free convection effects are negligibly small.

The thermal conductivity of lithium fluoride in the solid and the liquid state is shown in Fig. 4. The thermal conductivity ratio in the two states k_L/k_S is found to be equal to $1.0/3.0 = 0.66$ (the extrapolated value at the melting point is used for the solid). Turnbull (Ref. 2), using the derivation of Keyes (Ref. 3), calculates a value of 0.79 for the ratio of k_L/k_S for ionic solids. Turnbull's (Ref. 2) own analysis of the following liquids - $NaNO_3$, KNO_3, NaCl, $AgNO_3$, $KHSO_4$, $NaHSO_4$, NH_4HSO_4, KCNS, $ZnCl_2$ and NaOH gave a value of k_L/k_S in the range 0.71 to 0.99. The value of $k_L/k_S = 0.66$ obtained in this investigation compares favorably with the values reported in the literature.

Semi-theoretical expressions for the thermal conductivity of molten salts have been compiled by Gambill (Ref. 4). The correlations suggested are in terms of the density, molecular weight and the melting point of the molten salt.

$$k = 1.21\ T_m^{\frac{1}{2}} \rho_m^{\frac{2}{3}} / M^{\frac{7}{6}} \qquad 1$$

$$k = 0.75\ T_m^{\frac{1}{2}} \rho_m^{\frac{2}{3}} / M^{\frac{7}{6}} \qquad 2$$

For lithium fluoride

$T_m = 1143\,^{o}K$

$\rho_m = 1.8$ gm/cm^3

$M = 25.94$

Using these values, equation (1) gives a value of k = 1.36 BTU/hr ft F; equation (2) gives a value of k = 0.85 BTU/hr ft F. The measured value of k is 1.0 BTU/hr ft F. By using a constant of 0.9 instead of either 1.21 or 0.75, the thermal conductivity experimentally measured in this investigation can be correlated with its melting point, density and molecular weight. The correlating equation then becomes

$$k = 0.9\, T_m^{\frac{1}{2}} \rho_m^{\frac{2}{3}} / M^{\frac{7}{6}}$$

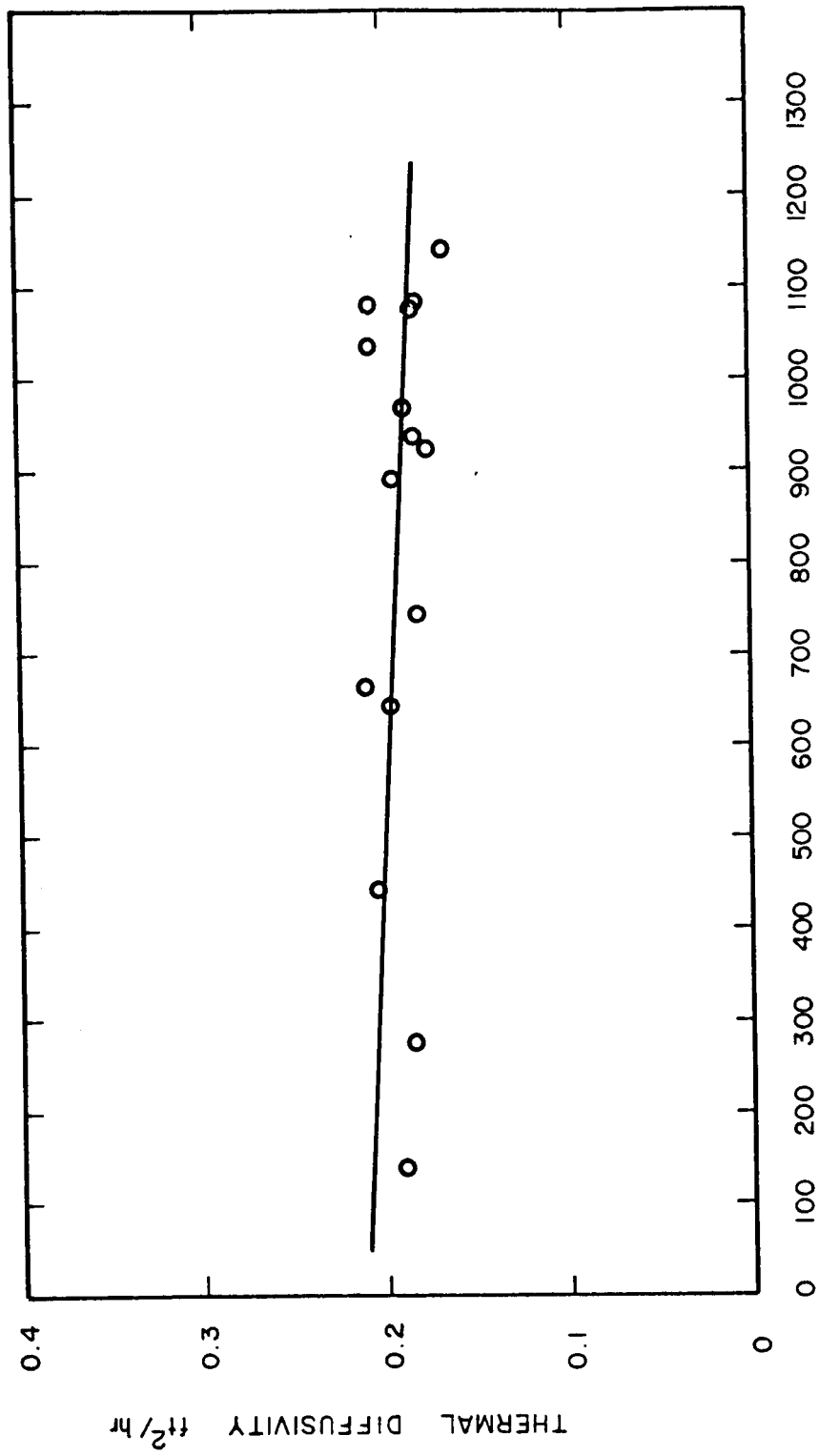

THERMAL DIFFUSIVITY OF BORON NITRIDE

FIG. 1

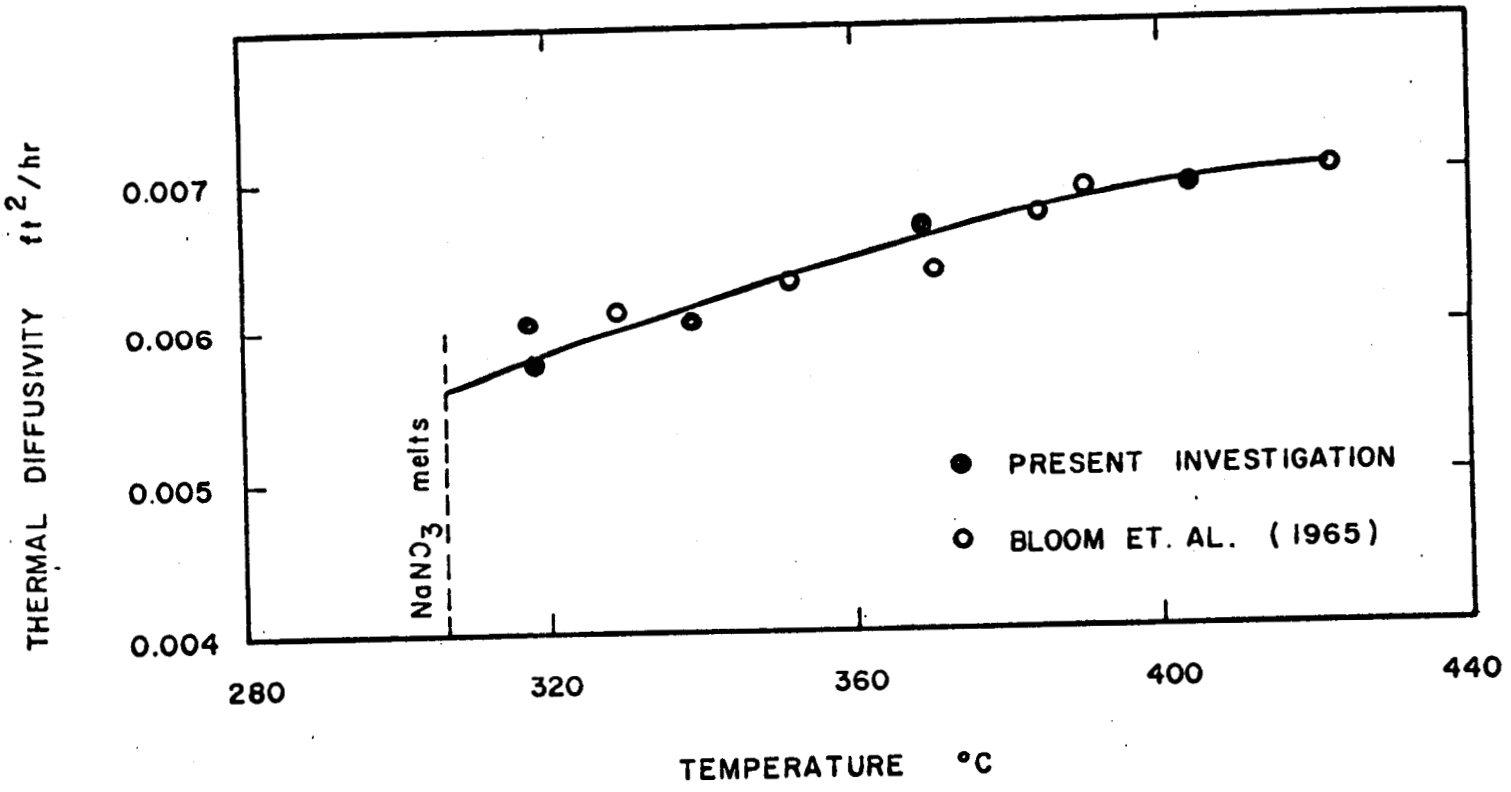

THERMAL DIFFUSIVITY OF SODIUM NITRATE

FIG. 2

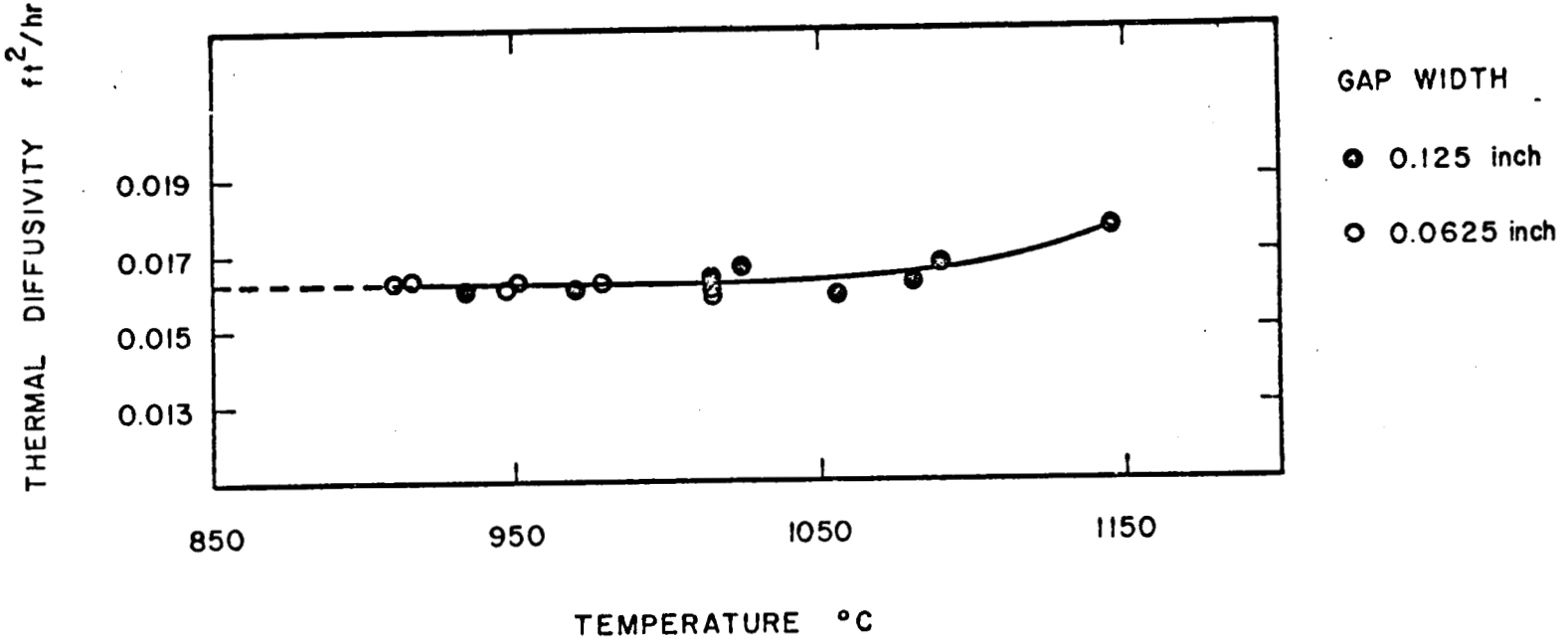

THERMAL DIFFUSIVITY OF LITHIUM FLUORIDE

FIG. 3

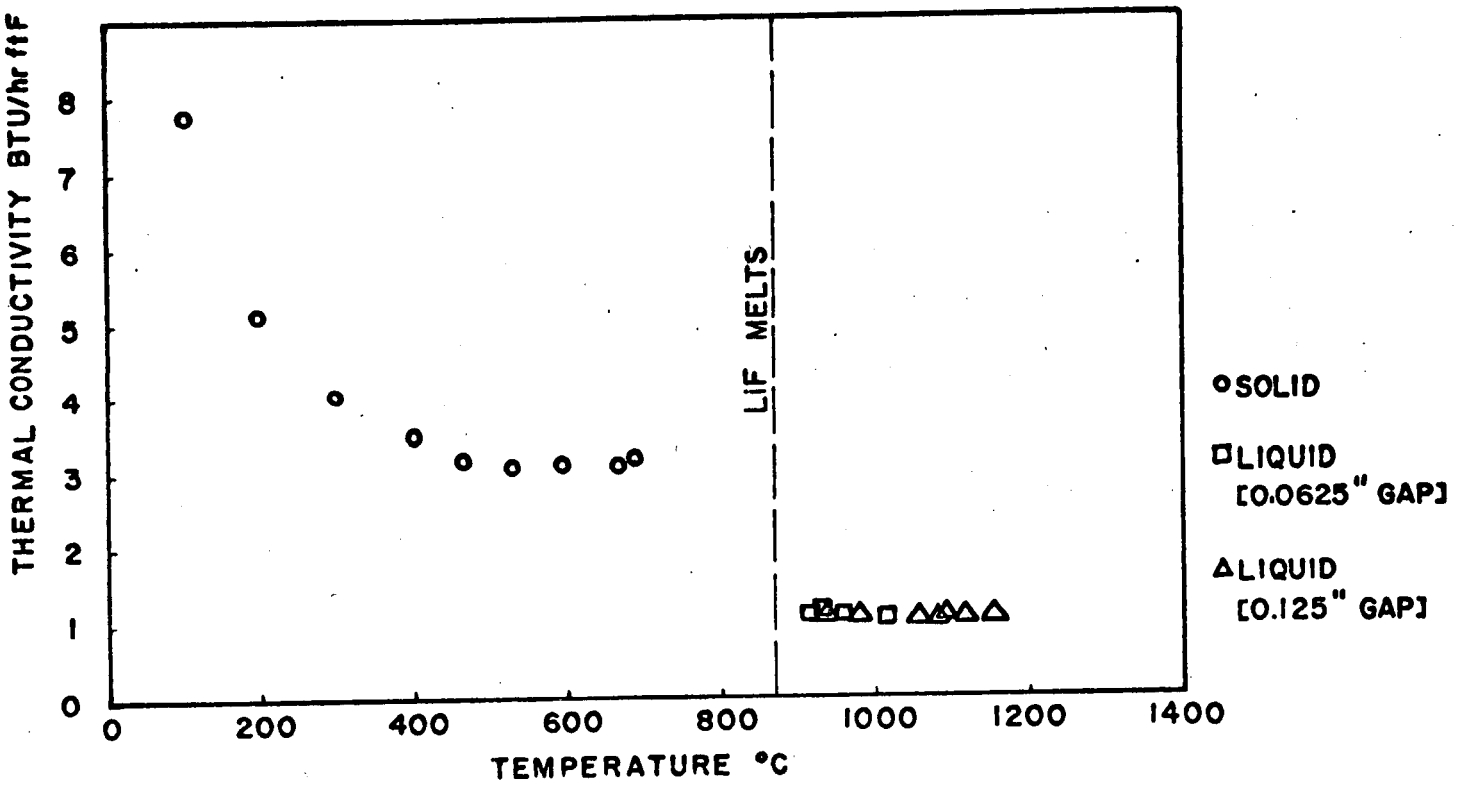

FIG. 4 — THERMAL CONDUCTIVITY OF LITHIUM FLUORIDE

High Temperature Thermal Diffusivity Measurement

Senior Investigator: Dr. Manfred Altman
Graduate Student: H. Keramaty

Thermal diffusivity of mixtures of Calcium Fluoride and Barium Fluoride was measured and reported in INDEC-SR-11.

The consecutive work on the diffusivity of Magnesium Fluoride, Calcium Fluoride and a mixture of the two is reported in Table (1) and Fig. (1).

More samples are necessary before a definite conclusion can be reached. The future work shall consist of the measurement of the thermal diffusivity of mixtures made of pressed powder of the components. This will give more control on the amount and distribution of each component of the mixture.

Some theoretical aspects are under study and shall be reported in future.

TABLE 1

Thermal Diffusivity of CaF_2, MgF_2, and their Mixtures

$\alpha \times 10^3$ (cm^2/sec)

Temp. (°C)	CaF_2	MgF_2	1/2 MgF_2 + 1/2 CaF_2
100	12.9	25.8	11.8
200	9.9	22.9	9.8
300	8.75	20.4	9.4
400	7.85	18.5	9.3
500	7.24	17.5	9.3
600	6.75	17.5	9.32
800	6.25	17.8	9.5
900	6.10	18.6	---
1000	6.13	--	---

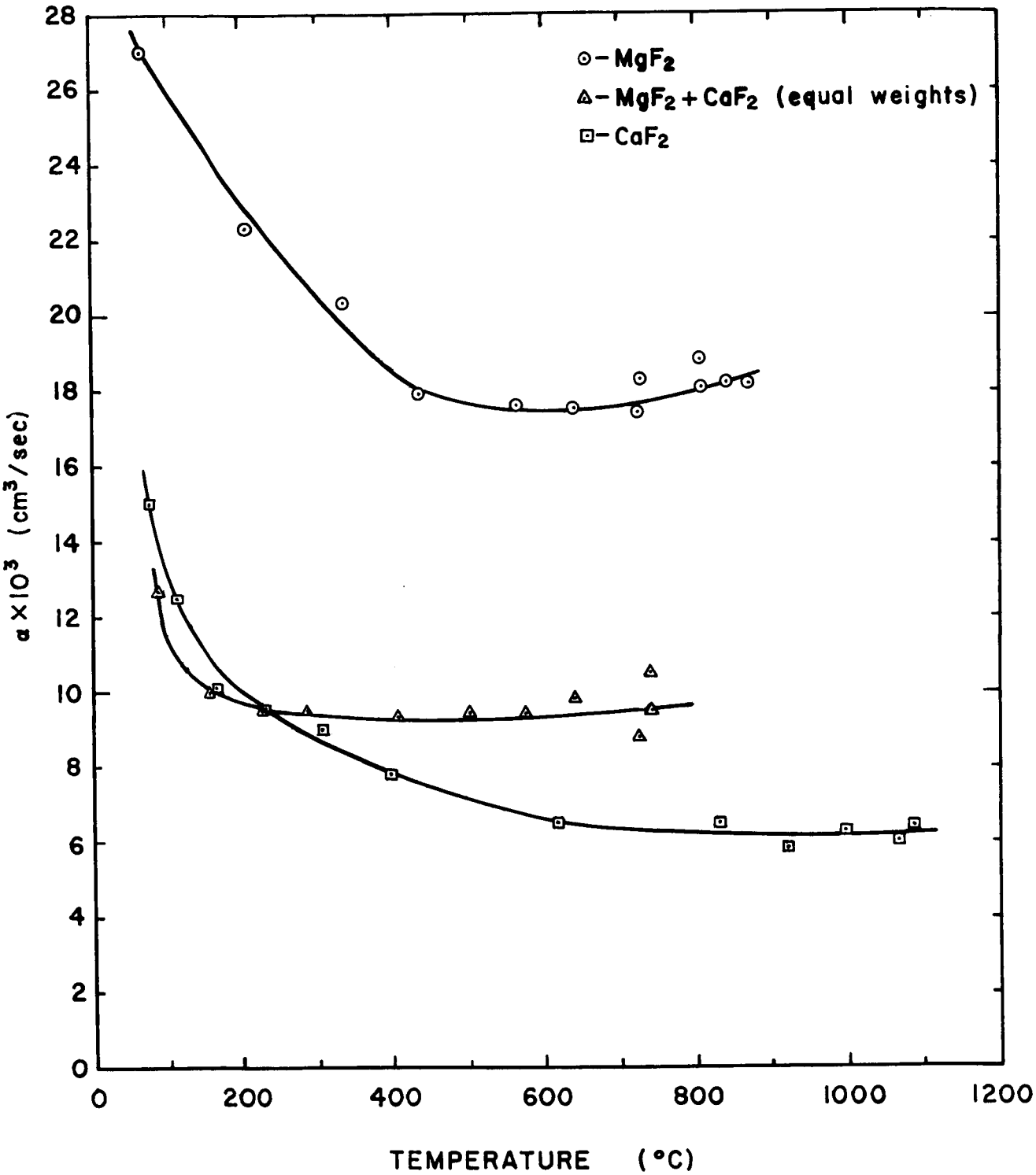

THERMAL DIFFUSIVITY OF CaF_2, MgF_2, AND THEIR MIXTURE

FIG. 1

Experimental Determination of the Thermoelectric Properties of Graphite Alloys

Senior Investigator: Dr. S. R. Pollack
Graduate Student: J. J. Curry

Due to the inavailability of graphite-compounds for study, we have begun an investigation of some quaternary chalcopyrite compounds belonging to the class I - II_2 - III - VI_4. Currently the investigation is centered on $CuCd_2In\ Te_4$.

The compound possesses a relatively high thermoelectric power on the order of 200μv/°K @ 300°K. It shows a p-type conductivity and has a resistivity of 6.35×10^{-2} ohm-cm.

Great difficulty was encountered in the reproducible fabrication of this compound. The stoichiometric weights of the constitutents are sealed in a vycor tube and slowly melted. The melt is held at temperature for 4 hours during which time it is mechanically agitated. It is then quenched to 0°C. The compound is then powdered and pressed to yield the desired shape for the samples. The samples are then sintered in vacuo and allowed to cool. The resultant samples are single phase and have reproducible electrical properties.

So far resistivity and thermoelectric power measurements have been made between 100°K and 300°K and the results are shown in Figure I. Although the thermoelectric power is quite high, the resistivity is also high.

It is not known whether the high resistivity is a result of low carrier concentration or low mobility. Hall coefficient studies will be made to delineate the nature of the resistivity. Unless the resistivity can be decreased through doping, it is apparent that $CuCd_2InTe_4$ would not be a practical thermoelectric material.

Equipment for the measurement of the resistivity, thermoelectric power and carrier concentration have been completed. They allow measurement of the above mentioned properties over the range 100°K to 400°K.

Apparatus for the measruement of the figure of merit between 300°K and 600°K is nearing completion. This apparatus is based on the method of Putley and Harman and is completely self contained.

Optical reflection measurements will be made as soon as the LRSM receives the equipment. These measurements should determine the optical band gap from the position of the absorption edge.

The thermoelectric properties are greatly dependent on the stoichiometry. In addition to the measurement of other compounds in this class, measurements will be on the system $CuCd_{2-x}In_{1+x}Te_4$.

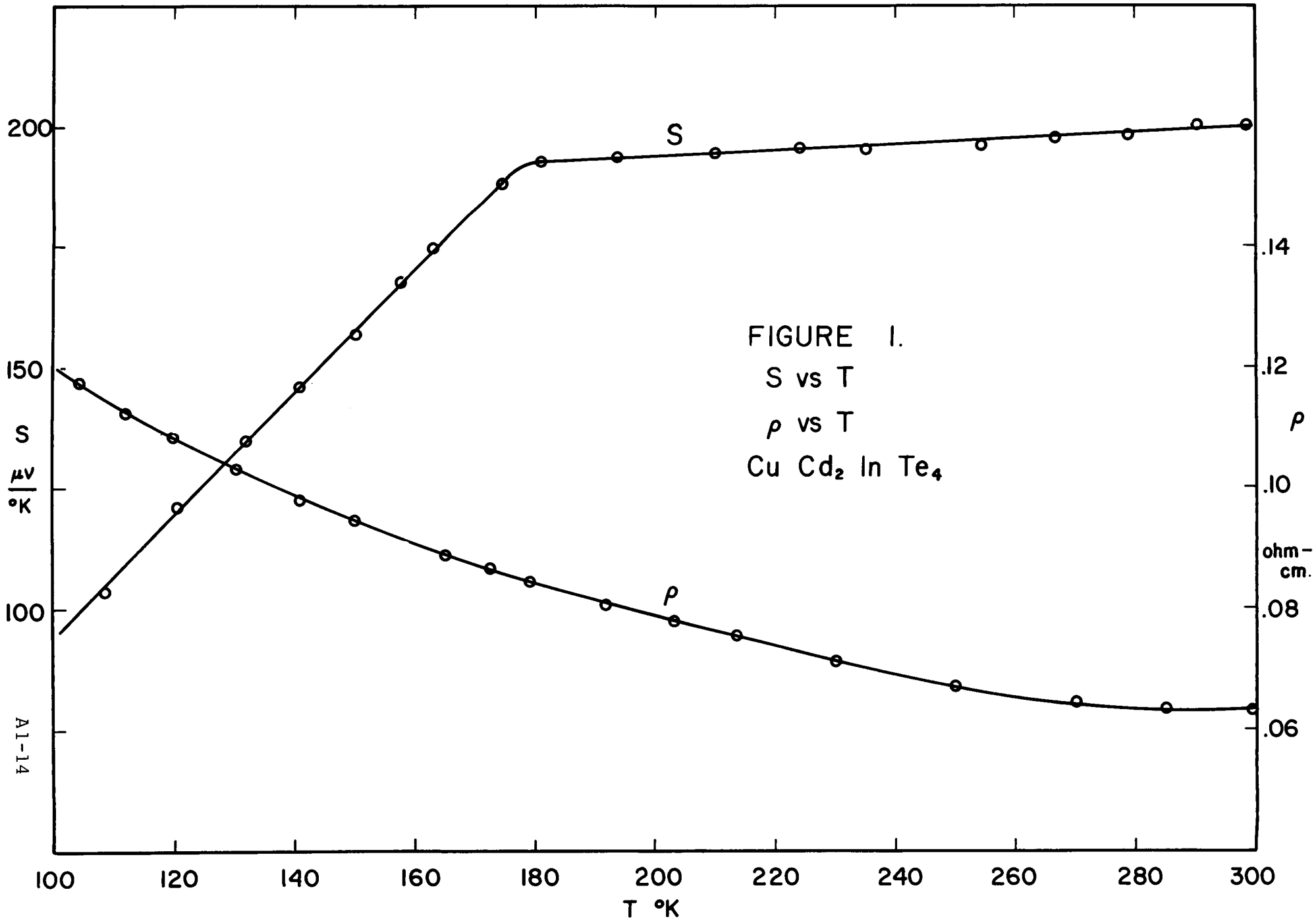

FIGURE 1.
S vs T
ρ vs T
Cu Cd_2 In Te_4

Tunnel Emission Cold Cathodes

Senior Investigator: Dr. S. R. Pollack

Graduate Student: S. Basavaiah

The description of vacuum system and other equipment and the method of sample preparation were given in the previous reports. A liquid nitrogen dewar system was built to take temperature dependent I-V data. Typical results and some explanations are given below.

Figure 1 shows a typical X-Y recorder plot of current vs voltage redrawn, at two different temperatures. The low voltage behavior of the same sample is given in Figure 2. It is to be noted that the junction is ohmic up to about 50 mV. Figure 3 shows the I-V plot of a sample having thicker oxide layer than the sample of Figure 1.

If the current transfer is mainly due to tunneling, very little temperature dependence of current is expected. On the other hand, if the current transfer is due to Schottky, emission current increases exponentially with temperature at a particular voltage. Figure 4 is a plot of ℓn I vs $V^{1/2}$ at two different temperatures. Figure 5 is a plot of ℓn I vs 1/T at a particular voltage.

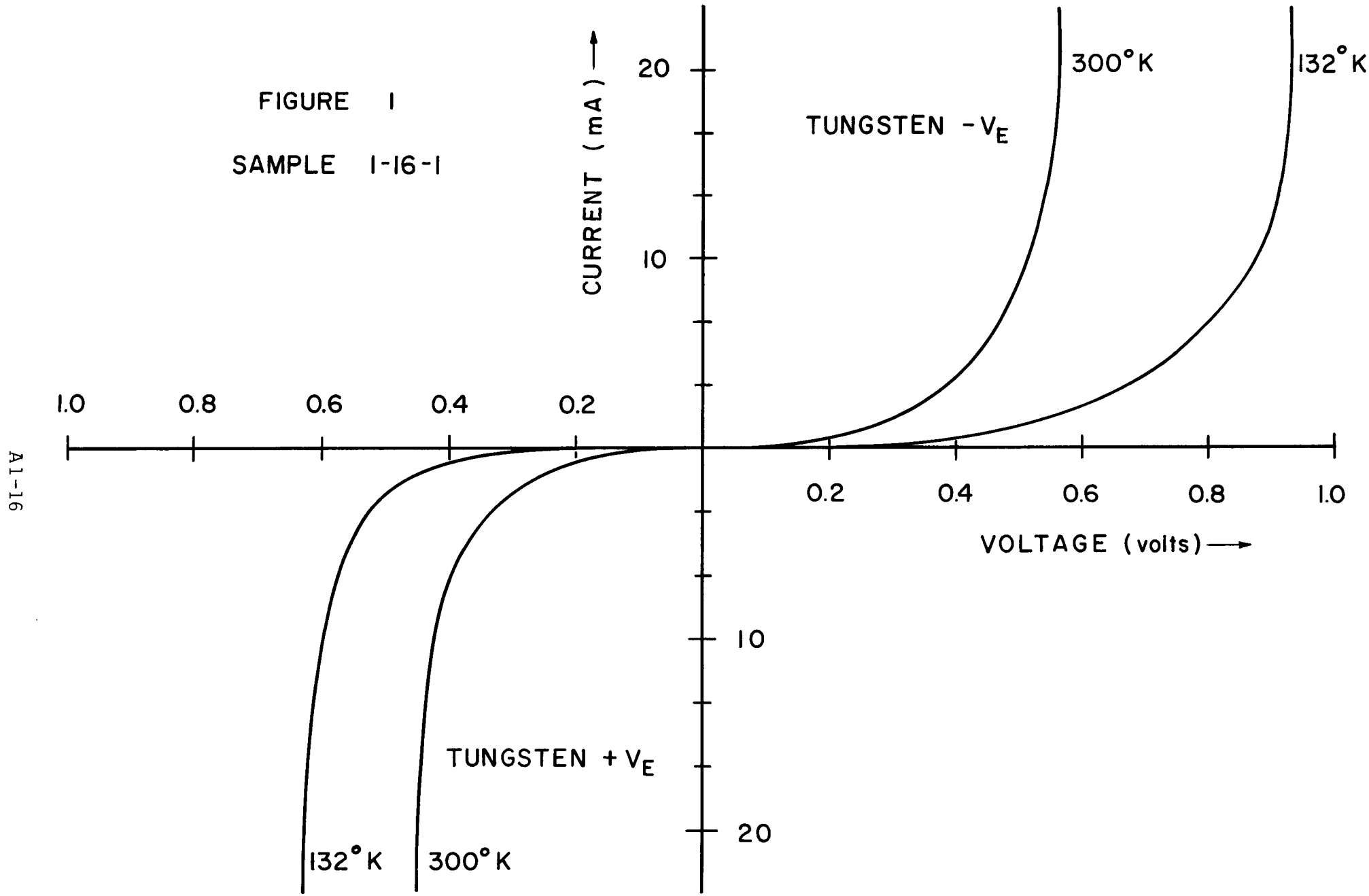
FIGURE 1
SAMPLE 1-16-1
CURRENT (mA)
20
10
300°K
132°K
TUNGSTEN -V_E
1.0
0.8
0.6
0.4
0.2
0.2
0.4
0.6
0.8
1.0
VOLTAGE (volts)
10
20
TUNGSTEN +V_E
132°K
300°K

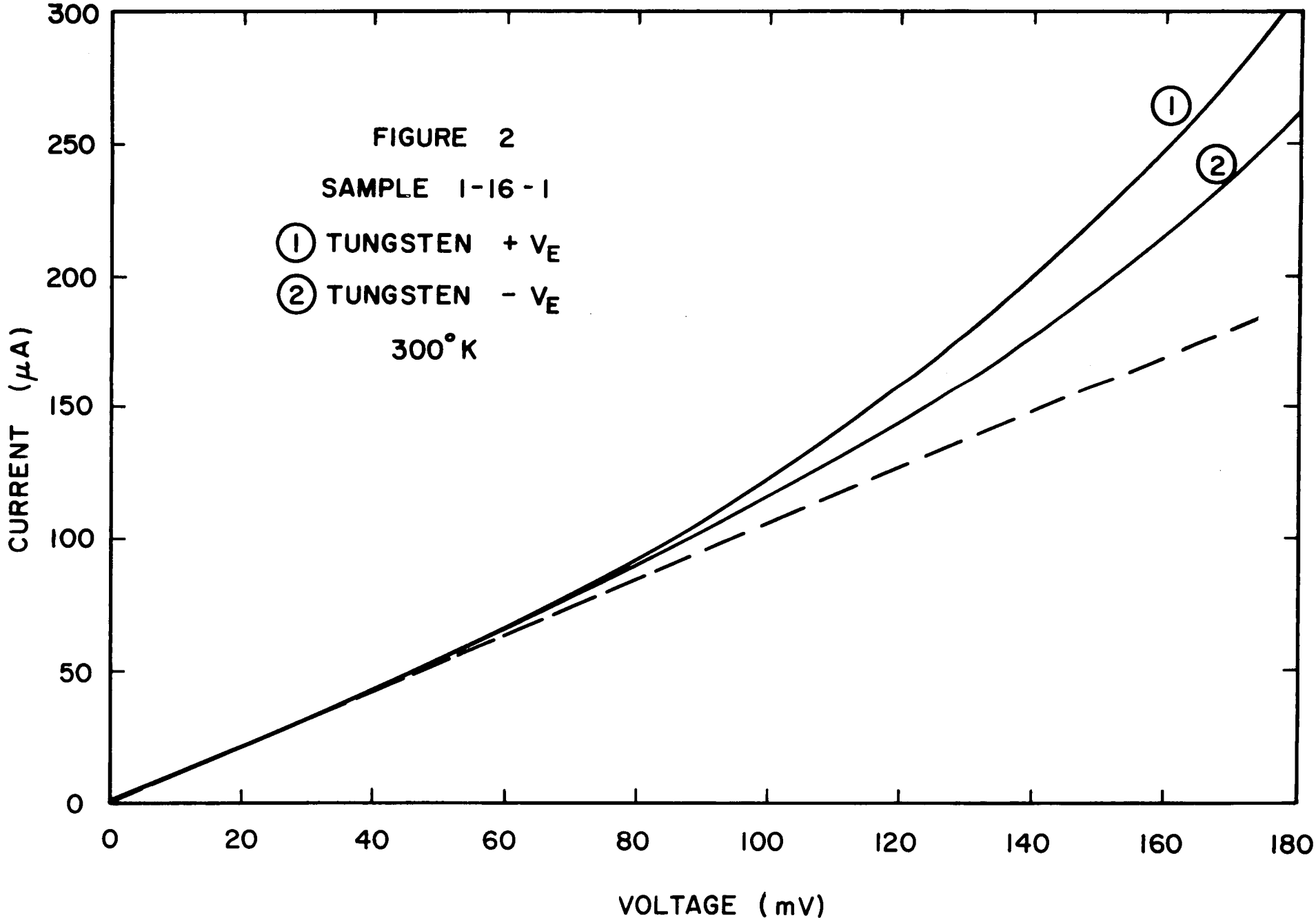
FIGURE 2
SAMPLE 1-16-1
① TUNGSTEN + V_E
② TUNGSTEN - V_E
300°K
CURRENT (μA)
VOLTAGE (mV)
0
50
100
150
200
250
300
0
20
40
60
80
100
120
140
160
180
①
②

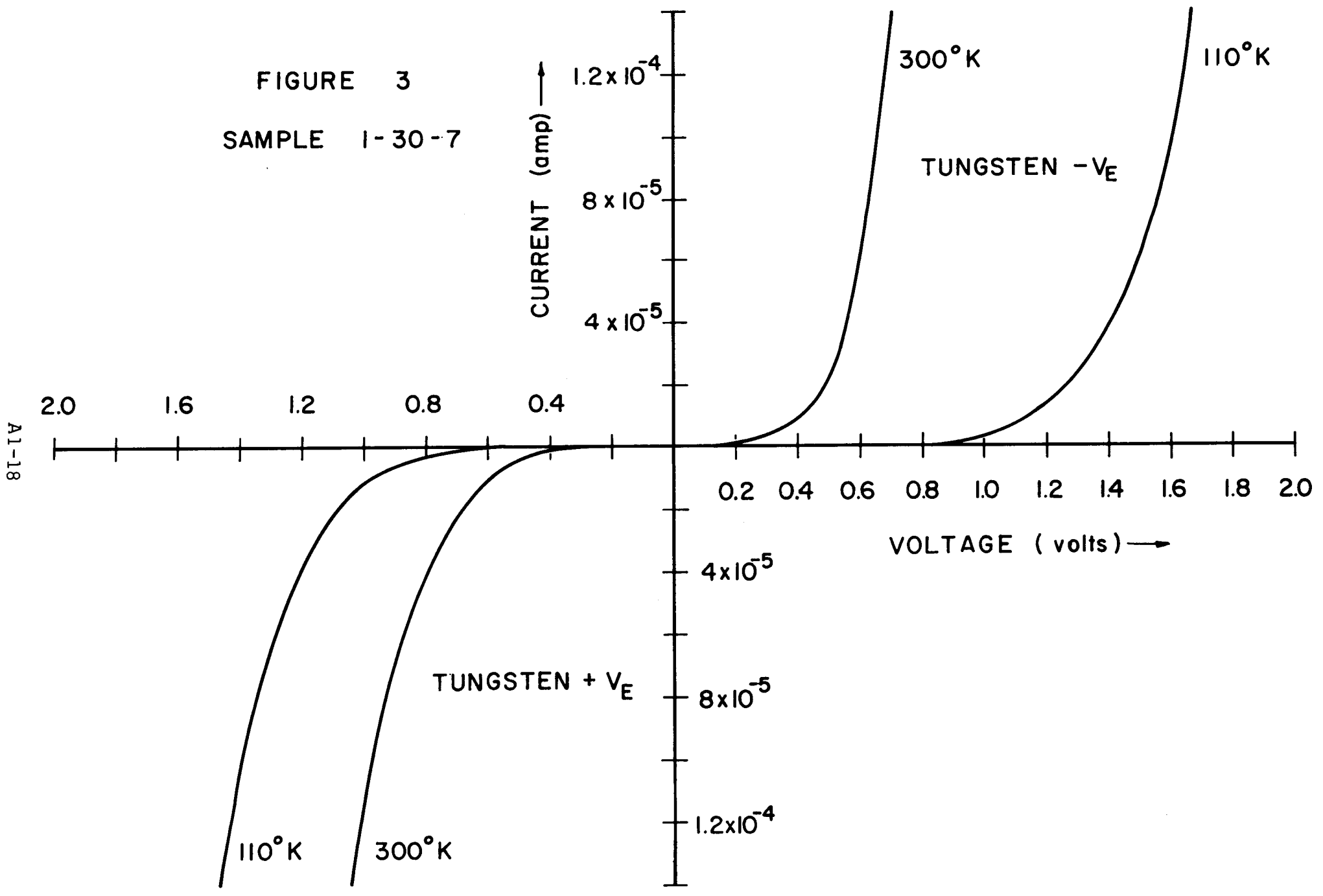
FIGURE 3
SAMPLE 1-30-7
CURRENT (amp) ⟶
1.2x10⁻⁴
8x10⁻⁵
4x10⁻⁵
2.0
1.6
1.2
0.8
0.4
0.2
0.4
0.6
0.8
1.0
1.2
1.4
1.6
1.8
2.0
VOLTAGE (volts) ⟶
300°K
110°K
TUNGSTEN −V_E
4x10⁻⁵
8x10⁻⁵
1.2x10⁻⁴
TUNGSTEN + V_E
110°K
300°K

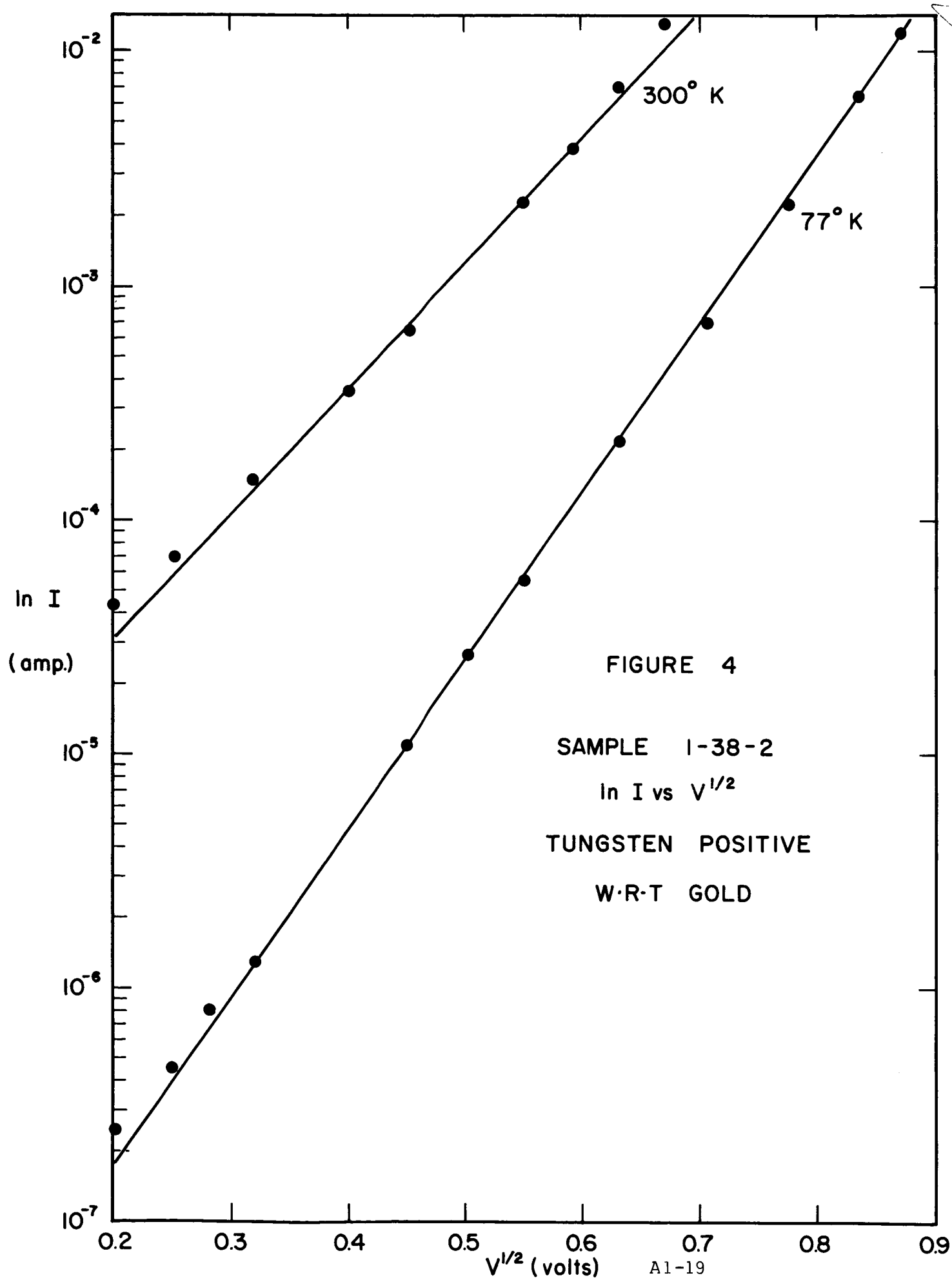

FIGURE 4

SAMPLE 1-38-2

ln I vs $V^{1/2}$

TUNGSTEN POSITIVE

W·R·T GOLD

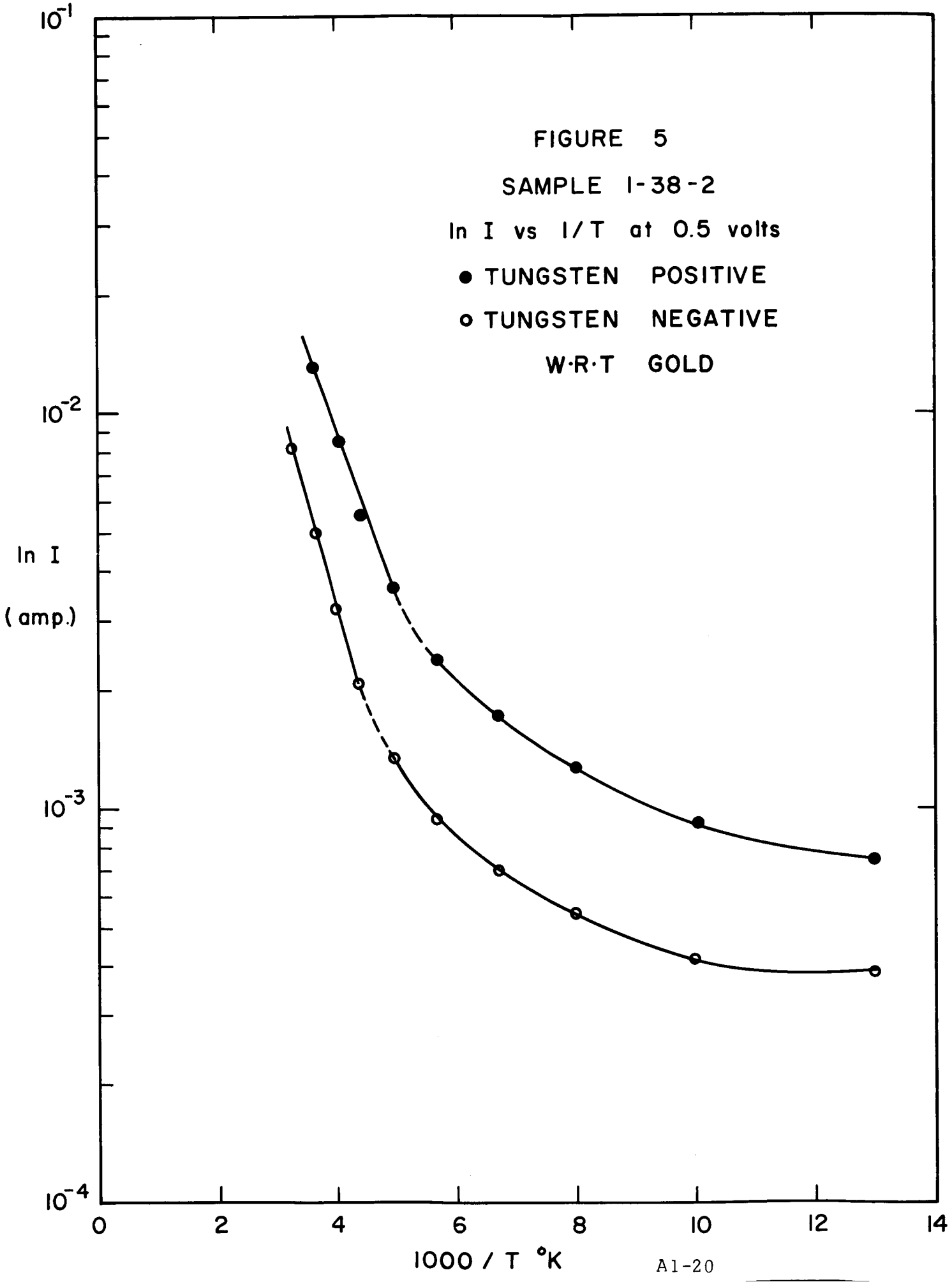
FIGURE 5
SAMPLE 1-38-2
In I vs 1/T at 0.5 volts
● TUNGSTEN POSITIVE
o TUNGSTEN NEGATIVE
W·R·T GOLD
10^{-1}
10^{-2}
10^{-3}
10^{-4}
In I
(amp.)
0
2
4
6
8
10
12
14
1000 / T °K

Studies of Thermal Transpiration for the Development of a "Thermal Pump"

Senior Investigator: Dr. Manfred Altman
Graduate Student: E. Hopfinger

The phenomenon of thermal transpiration was described in the previous reports, and flow rates through an infinitely thin membrane, calculated from kinetic theory, as well as graphs characteristic of flow rates through membranes of finite thickness, have been presented.

The phenomenon of thermal transpiration is a coupled flow system and is governed by the equations of non-equilibrium thermodynamics. When higher order terms in the affinities are neglected, we have

(1) $$y_1 = L_{11} X_1 + L_{12} X_2$$ Energy flux

(2) $$y_2 = L_{21} X_1 + L_{22} X_2$$ Particle flux

where X_1 and X_2 are the affinities, which can be expressed as

(3) $$X_1 = -\frac{1}{T^2}\frac{dT}{dz}\,; \qquad X_2 = -\frac{d}{dz}\left(\frac{\mu}{T}\right)$$

$$= -R\frac{d\ln p}{dz} + H\frac{1}{T^2}\frac{dT}{dz}$$

where R is the gas constant

H the molar enthalpy of the gas

P the pressure

T the temperature.

Substitute equation (3) in equations (1) and (2) and rearrange

(4) $$y_1 = (L_{12}H - L_{11})\frac{1}{T}\frac{d\ln T}{dz} - L_{12}R\frac{d\ln p}{dz}$$

(5) $$y = (L_{12}H - L_{11})\frac{1}{T}\frac{d\ln T}{dz} - L_{12}R\frac{d\ln p}{dz}$$

where Onsager's relation

(6) $$L_{12} = L_{21}$$

has been used.

The L's are coefficients and can be obtained directly from experiments or expressed in terms of characteristic parameters of the porous medium by choosing an adequate model and utilizing microscopic theories. A model utilized by reference (1) visualizes the porous medium as a collection of "dust" particles which are then considered as giant molecules fixed in space. This model makes it possible to use the formal equations for binary diffusion. A viscous term is added to the expressions obtained from the diffusion equations and the total expression for the flow of gases (moles sec^{-1} and unit area) is

(7) $$y = -\frac{PD_K}{RT}\left[\left(1+\frac{B_0 p}{\nu D_K}\right)\frac{d\ln p}{dz} - \left(\frac{\alpha_Q n_d RT}{p+2\alpha_Q n_d RT}\right)\frac{d\ln T}{dz}\right]$$

By comparison of equation (5) with (7), the L's can be expressed in terms of D_K the Knudsen permeability, B_o a geometry factor, ν the gas viscosity, and $\alpha_Q n_d RT$ a term containing the thermal diffusion coefficient α_Q and number density of the "dust" particles.

(8) $$\alpha_Q n_d RT = \frac{3}{4}\frac{\nu}{M}\left(\frac{\epsilon/q}{D_K}\right)RT$$

where M is molecular weight of gas

ϵ/q porosity-tortuosity factor.

Differential approximation

(9) $$\frac{dT}{dz} \approx \frac{\Delta T}{l}$$

Then for $y_2 = 0$

(10) $$\frac{\Delta p}{\bar{p}} = \left[\frac{\alpha_Q n_d RT(\nu D_K/B_0)}{(\bar{p}+2\alpha_Q n_d R\bar{T})(\bar{p}+\nu D_K/B_0)}\right] \frac{\Delta T}{\bar{T}}$$

The maximum of Δp is found to be

(11) $$\Delta p_{max} = \frac{\alpha_Q n_d RT\,(\nu D_K/B_0)}{[(2\alpha_Q n_d RT)^{\frac{1}{2}} + (\nu D_K/B_0)]^2} \frac{\Delta T}{\bar{T}}$$

and its position is at

(12) $$p_{max} = \sqrt{2\alpha_Q n_d RT \frac{\nu D_K}{B_0}}$$

The expression for the flow coefficient in the case of $\Delta p = 0$ is

(13) $$\frac{y_2 l}{\Delta T} = \frac{\bar{p} D_K}{R\bar{T}^2} \left(\frac{\alpha_Q n_d R\bar{T}}{\bar{p}+2\alpha_Q n_d R\bar{T}}\right)$$

The values of D_K and B_o or $\nu D_K/B_o$ are obtained from isothermal permeability experiments and the value of $\alpha_Q n_d RT$ from steady state thermal transpiration runs using equation (11).

Isothermal permeability graphs are presented in Figure 1 and 2 for Helium and Argon in porous ceramics Selas 06 and 02.

Steady state thermal transpiration plots for He and Ar in the same samples are presented in Figure 3.

The porous ceramics specifications are listed in Table I and the values of the parameters needed for the dusty-gas theory equations are listed in Table II.

Table I. Specifications of porous ceramics Selas 06 and 02.

Membrane	Area (cm^2)	Thickness (cm)	Porosity† %	Average† pore diam. ($cm \times 10^4$)	Average * pore diam. ($cm \times 10^4$)
Selas 06	38.5	.525	58	.35	.39
Selas 02	38.5	.608	59	.85	1.49

*Calculated from permeability values following the method suggested by ref. ( ).

†Specified by manufacturer.

Table II. Parameters required for the dusty-gas theory equations.

System	D_K ($cm^2\ sec^{-1}$)	$D_K\ \nu/B_o$ (cm Hg)	ν (poise $\times 10^4$)	B_o ($cm^2 \times 10^{11}$)	$\alpha_Q n_d RT$ (cm Hg)	ϵ/q *
He in Selas 06	.117	210	2.02	.84	20.8	.028
Ar in Selas 06	.038	73.2	2.26	.88	4.0	.014
He in Selas 02	1.27	115	2.0	16.80	11.6	.185
Ar in Selas 02	.415	42.2	2.26	16.68	2.0	.088

* ϵ/q is according to theory only a geometry factor; it is, however, seen here that it also depends on the gas.

Differential approximation

$$\frac{dT}{dz} \approx \frac{\Delta T}{l} \tag{9}$$

Then for $y_2 = 0$

$$\frac{\Delta p}{\bar{p}} = \left[\frac{\alpha_Q n_d RT(\nu D_K/B_Q)}{(\bar{p}+2\alpha_Q n_d R\bar{T})(\bar{p}+\nu D_K/B_Q)}\right] \frac{\Delta T}{\bar{T}} \tag{10}$$

The maximum of Δp is found to be

$$\Delta p_{max} = \frac{\alpha_Q n_d RT\,(\nu D_K/B_Q)}{[(2\alpha_Q n_d RT)^{\frac{1}{2}} + (\nu D_K/B_Q)]^2} \frac{\Delta T}{\bar{T}} \tag{11}$$

and its position is at

$$p_{max} = \sqrt{2\alpha_Q n_d RT \frac{\nu D_K}{B_Q}} \tag{12}$$

The expression for the flow coefficient in the case of $\Delta p = 0$ is

$$\frac{y_2 l}{\Delta T} = \frac{\bar{p} D_K}{R\bar{T}^2} \left(\frac{\alpha_Q n_d R\bar{T}}{\bar{p}+2\alpha_Q n_d R\bar{T}}\right) \tag{13}$$

The values of D_K and B_o or $\nu D_K/B_o$ are obtained from isothermal permeability experiments and the value of $\alpha_Q n_d RT$ from steady state thermal transpiration runs using equation (11).

Isothermal permeability graphs are presented in Figure 1 and 2 for Helium and Argon in porous ceramics Selas 06 and 02.

Steady state thermal transpiration plots for He and Ar in the same samples are presented in Figure 3.

The porous ceramics specifications are listed in Table I and the values of the parameters needed for the dusty-gas theory equations are listed in Table II.

Table I. Specifications of porous ceramics Selas 06 and 02.

Membrane	Area (cm^2)	Thickness (cm)	Porosity† %	Average† pore diam. ($cm \times 10^4$)	Average * pore diam. ($cm \times 10^4$)
Selas 06	38.5	.525	58	.35	.39
Selas 02	38.5	.608	59	.85	1.49

*Calculated from permeability values following the method suggested by ref. ( ).

†Specified by manufacturer.

Table II. Parameters required for the dusty-gas theory equations.

System	D_K ($cm^2\ sec^{-1}$)	$D_K\ \nu/B_o$ (cm Hg)	ν (poise $\times 10^4$)	B_o ($cm^2 \times 10^{11}$)	$\alpha_Q n_d RT$ (cm Hg)	ϵ/q *
He in Selas 06	.117	210	2.02	.84	20.8	.028
Ar in Selas 06	.038	73.2	2.26	.88	4.0	.014
He in Selas 02	1.27	115	2.0	16.80	11.6	.185
Ar in Selas 02	.415	42.2	2.26	16.68	2.0	.088

* ϵ/q is according to theory only a geometry factor; it is, however, seen here that it also depends on the gas.

Table II lists all the parameters needed for the calculation of the flow coefficients from equation (13). In Figure 4, these calculated flow coefficients (flow rate in ml sec^{-1} multiplied by thickness and divided by area and temperature difference) and presented as solid lines and the points are measured values. Clearly the theory agrees satisfactorily with experiments.

The efficiency of the system is expressed as

$$\eta = \frac{\text{Output}}{\text{Heat Input}} \tag{14}$$

The power output is head times flow rate and the heat input is obtained from the electrical power input. Figure 5 and 6 show plots of head versus flow rates and efficiency versus flow rates for Helium in the two porous ceramics at $\Delta T = 105^{\circ}$ C. The maximum efficiency is at one half of the maximum flow rate and it has a value of 3.3×10^{-3}% in the 02 ceramics. This value could reach 5×10^{-2} to 10^{-1}% or higher values in a membrane of very uniform pore structure (large values of ϵ/q), high porosity and low thermal conductivity.

In order to draw sound conclusions, other membranes have to be tested and such experiments are in progress.

REFERENCES

(1) E. A. Mason, R. B. Evans III, and G. M. Watson, J. Chem. Phys. 38, 1808 (1963)

(2) Carman, Proc. Roy. Soc. A, 203, 55 (1950)

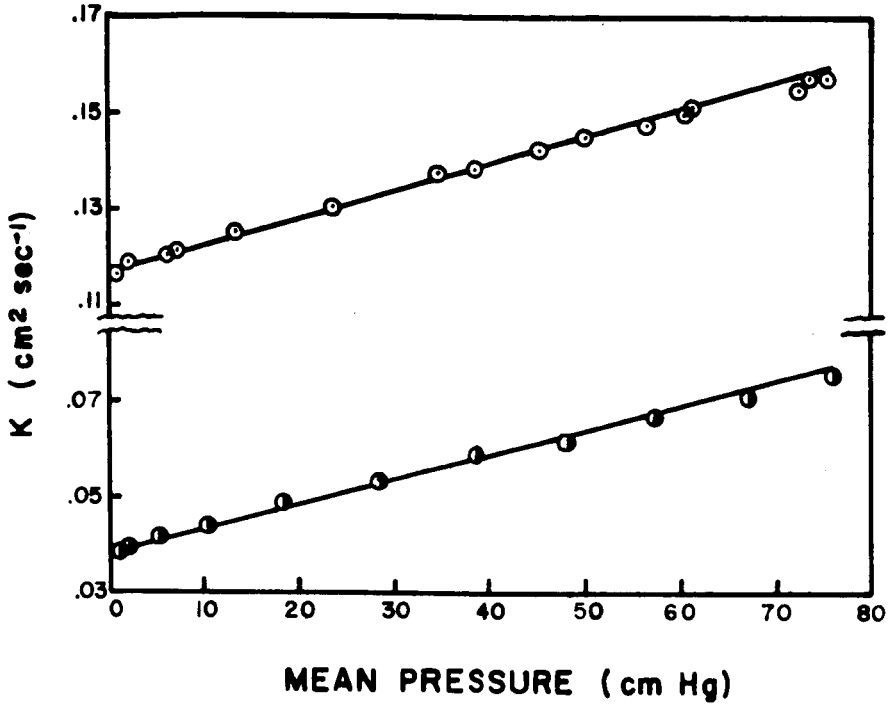

Fig. 1. Isothermal permeabilities as a function of pressure for He(O) and Ar(◑) in pourous ceramics Selas #06 at 27°C.

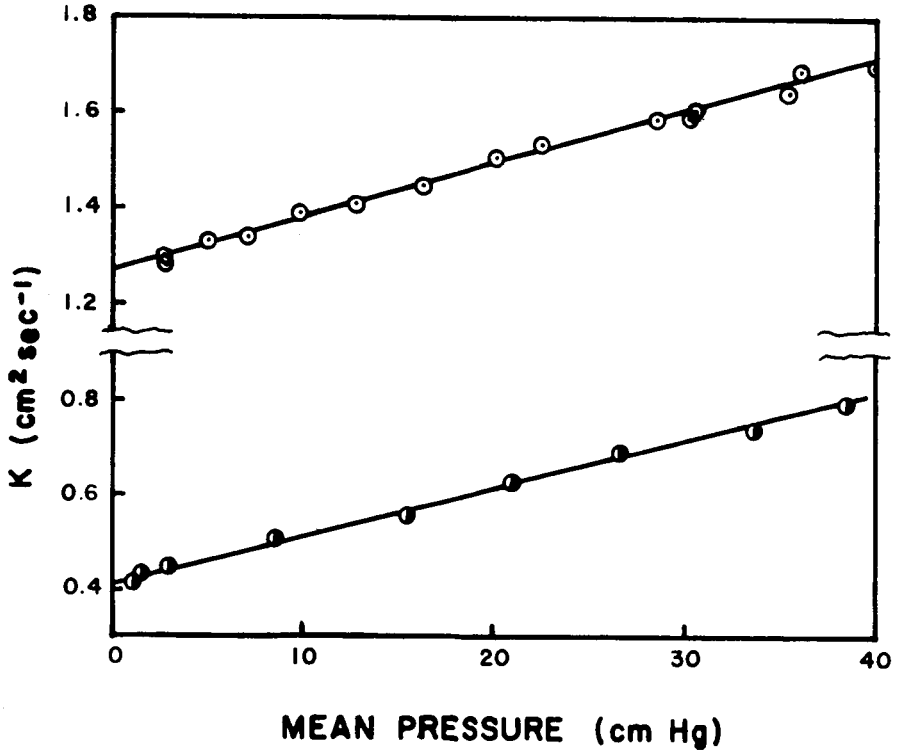

Fig. 2. Isothermal permeabilities as a function of pressure for He(O) and Ar(◑) in a pourous ceramics, Selas #02 at 24°C.

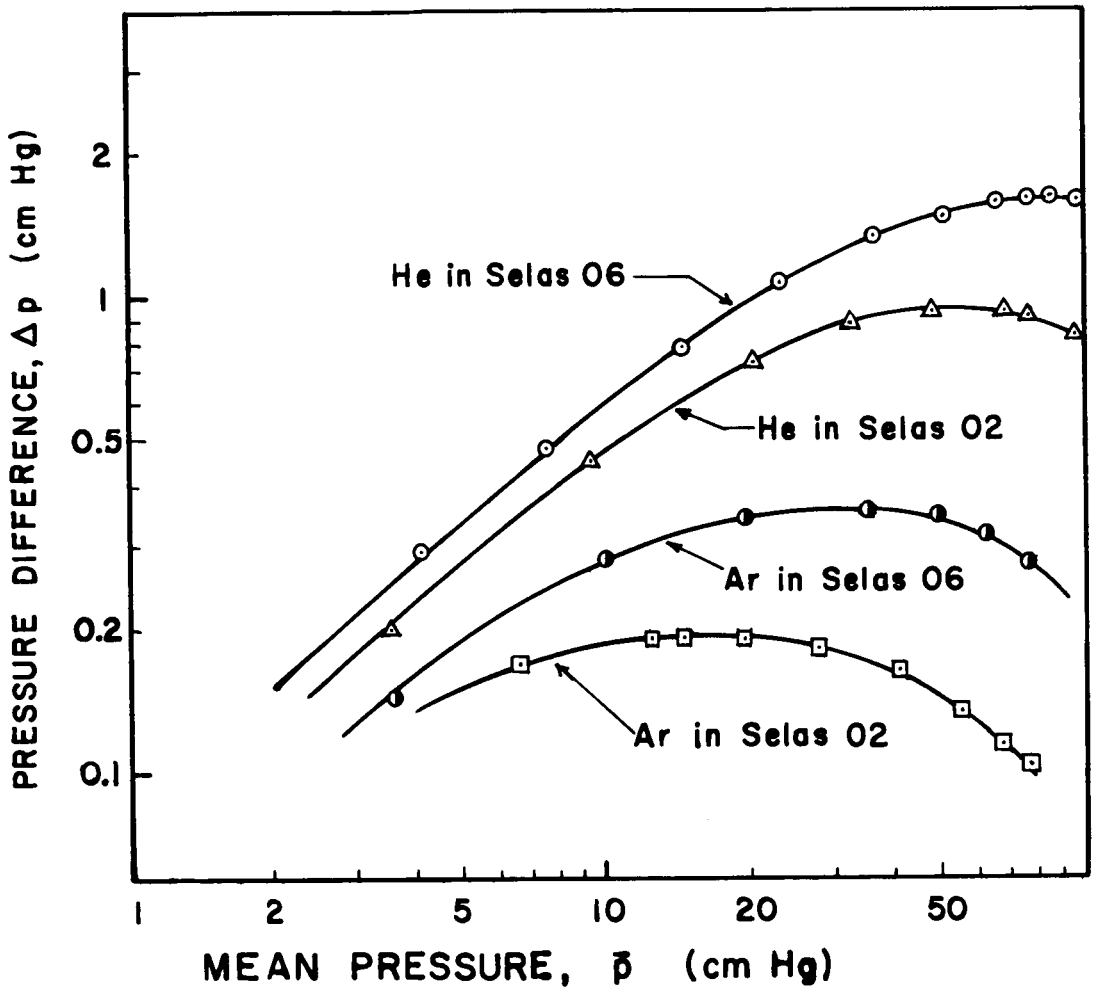

Fig. 3. Thermal transpiration plots in porous ceramics Selas #06 and #02 for He and Ar; $\bar{T} = 360^{o}K$; $R^2 = 1.160$

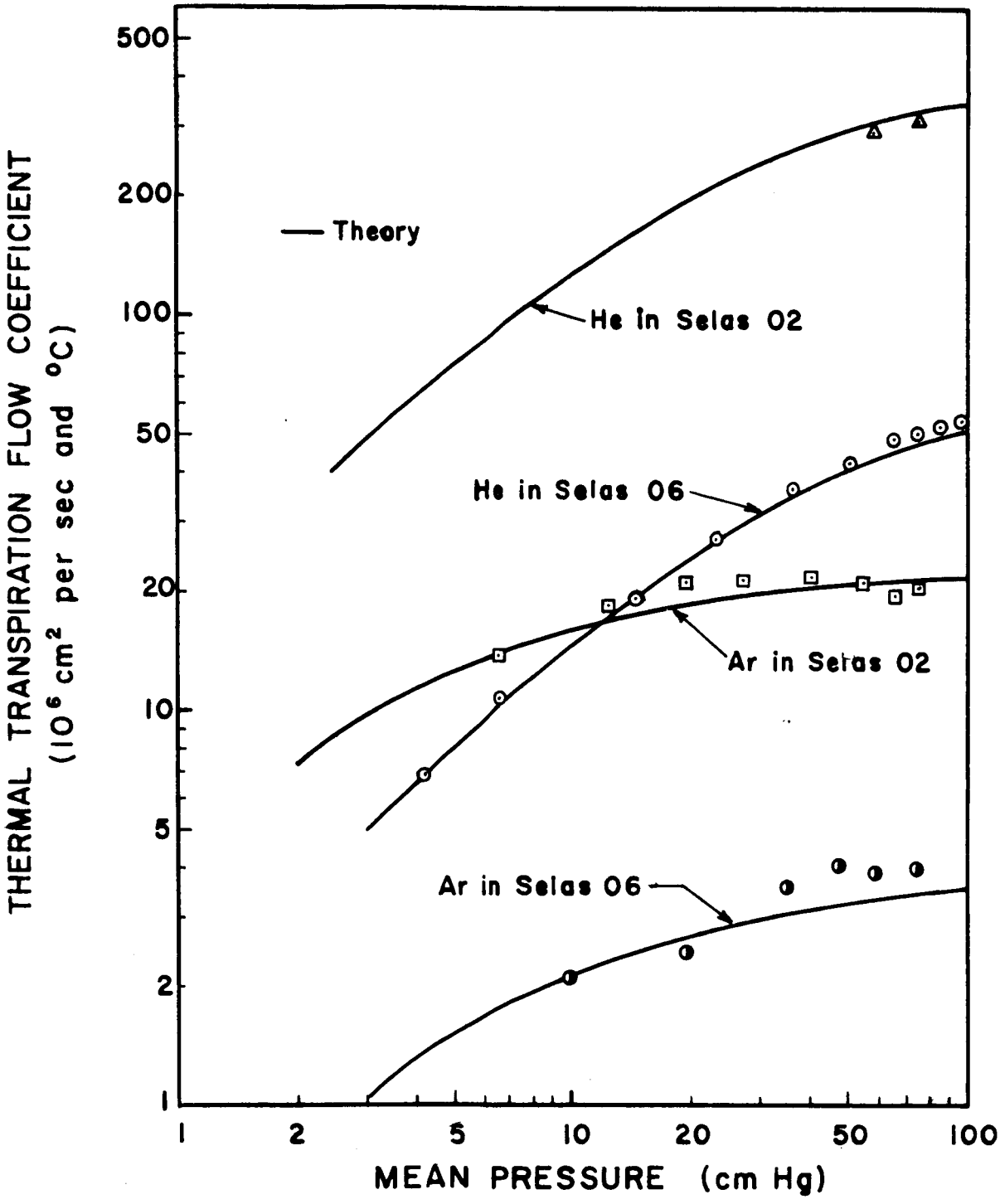

Fig. 4. Thermal transpiration flow coefficient of porous ceramics Selas #06 and #02 for He and Ar at $\bar{T}$ = 360°K.

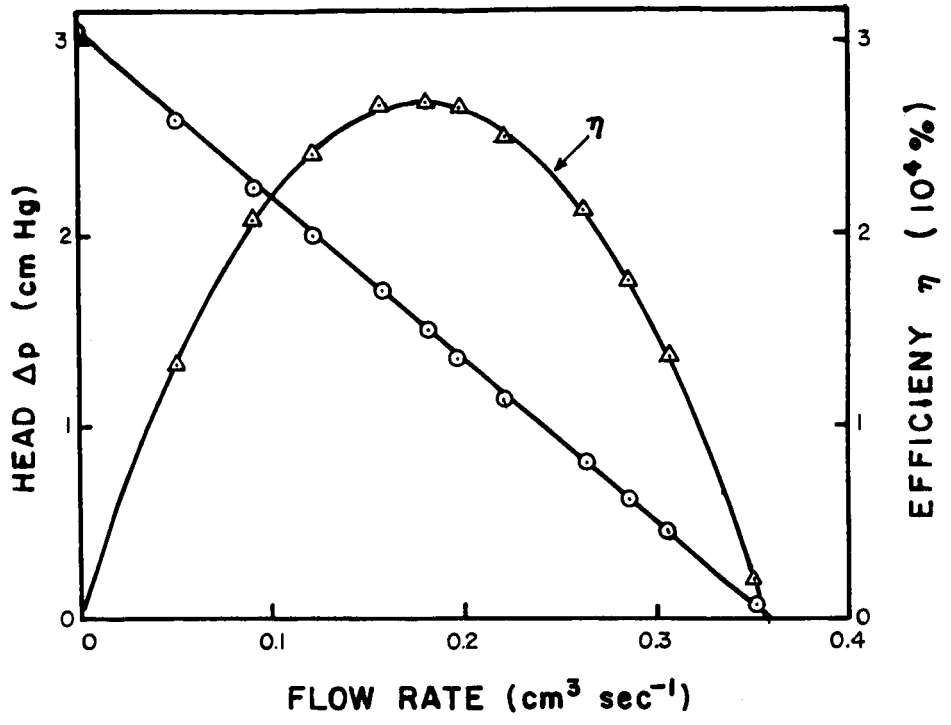

Fig. 5. Head vs. flow rate and pumping efficiency of He in porous ceramics #06. $\bar{T}$= 400°K; R_0^2= 1.30; $\bar{P}$ = 1 atm.

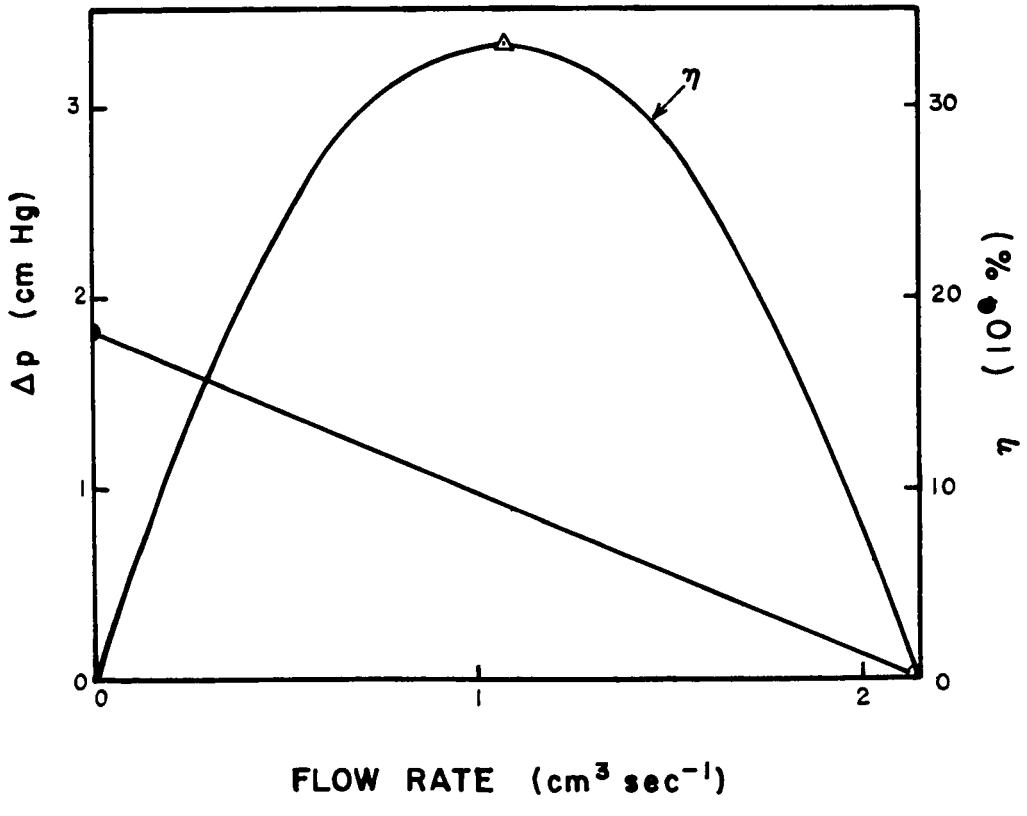

Fig. 6. Head vs. flow rate and pumping efficiency of He in porous ceramics #02. $\bar{T}$ = 374°K; R_0^2 = 1.328; $\bar{P}$ = 1 atm.

PLASMA ENGINEERING

APPENDIX

A-2

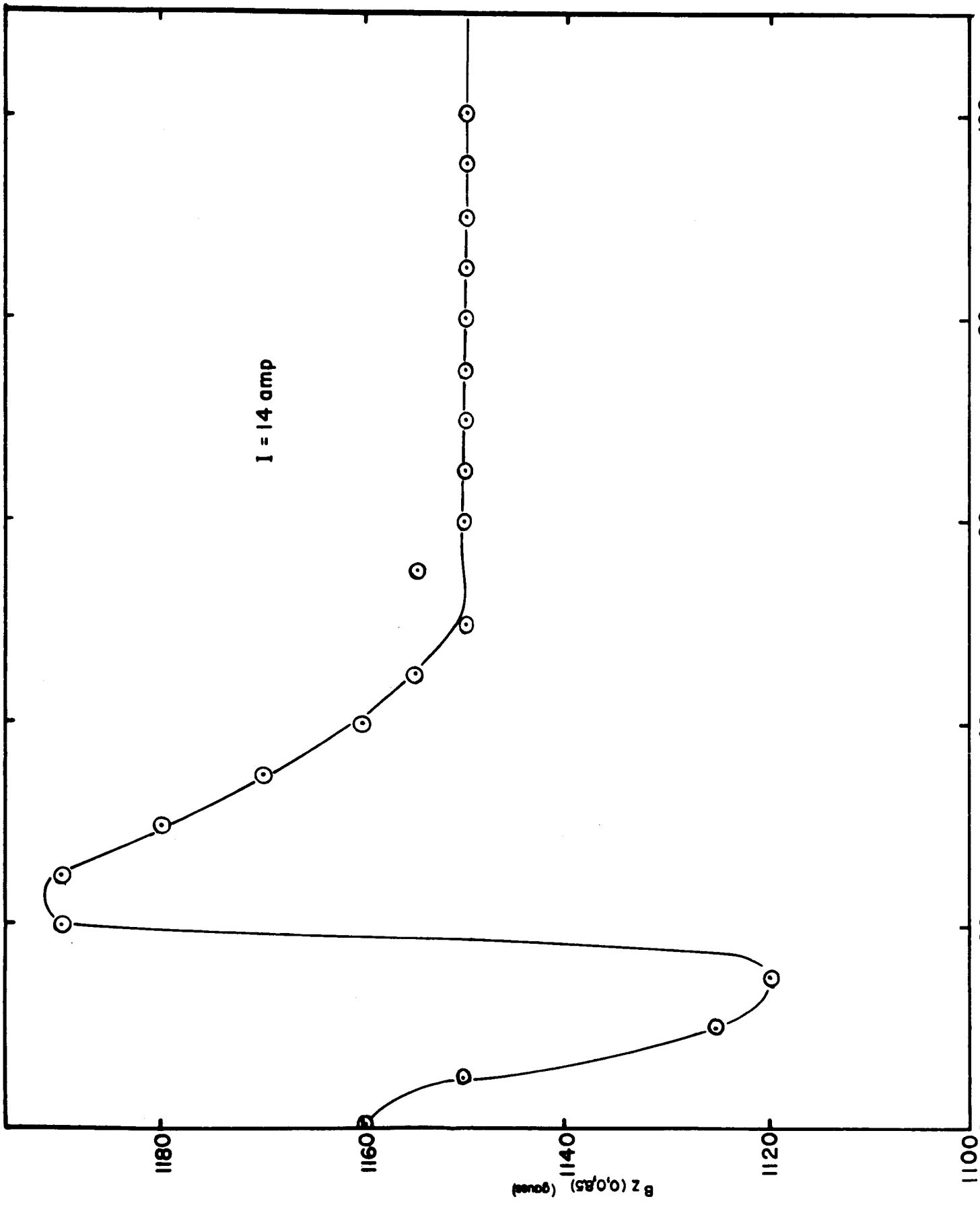

TIME DEPENDENCE OF Z COMPONENT OF THE MAGNETIC FIELD
Fig. 1

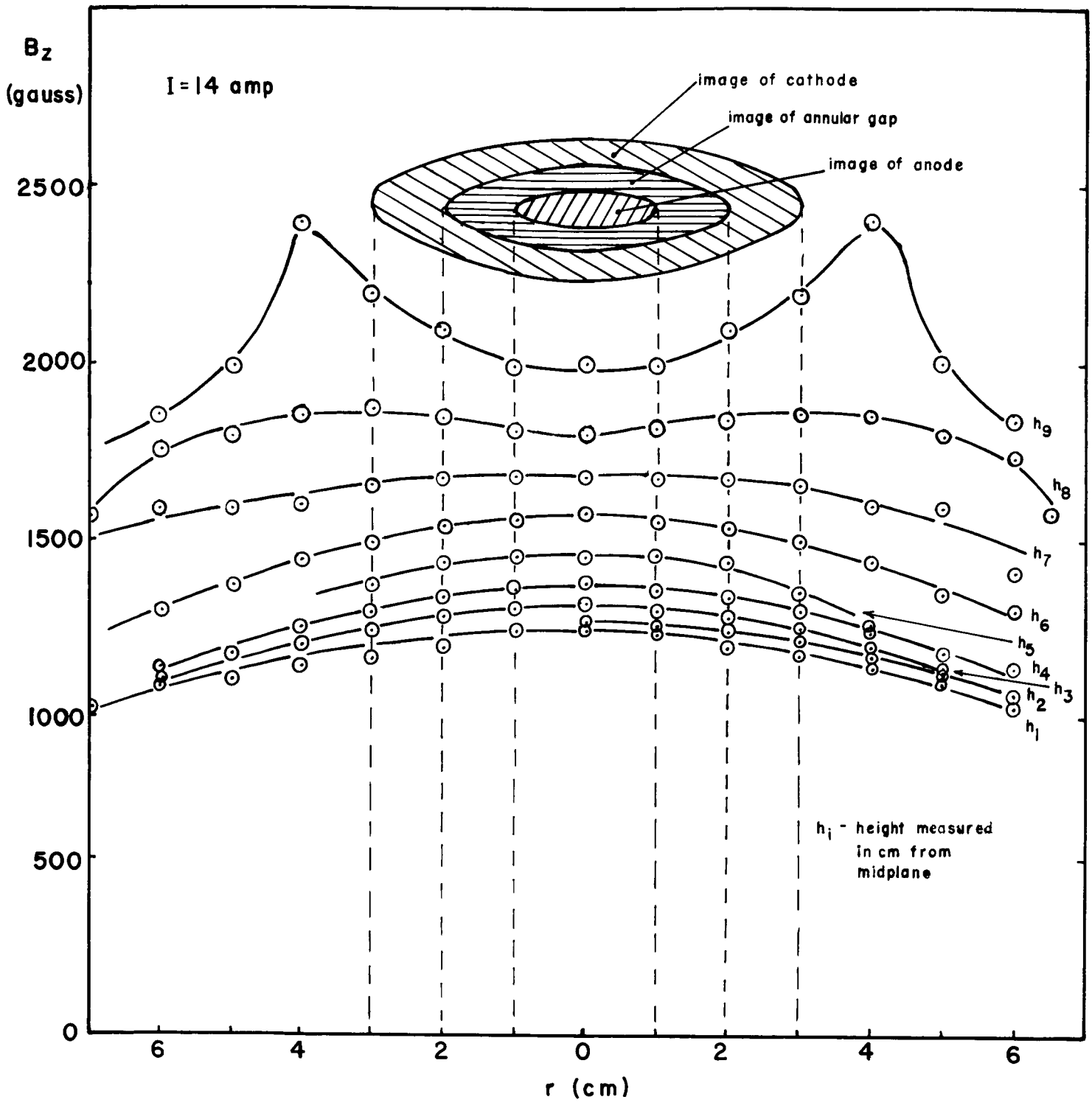

B_z AS A FUNCTION OF r AT VARIOUS z=CONSTANT PLANES MEASURED IN CM. ABOVE MIDPLANE BETWEEN POLE FACES

Fig. 2

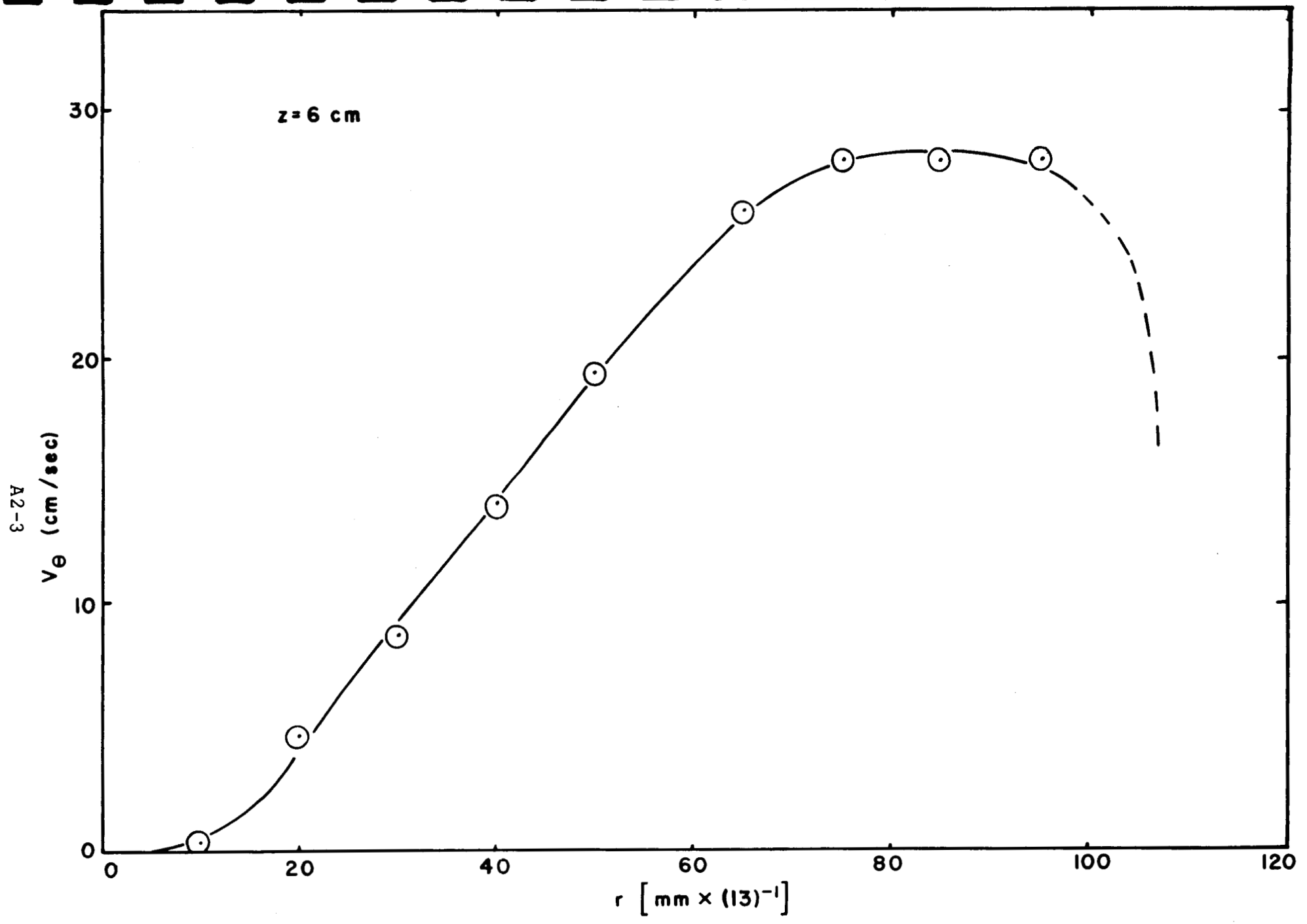

VARIATION OF V_e AS A FUNCTION OF r.

Fig. 3

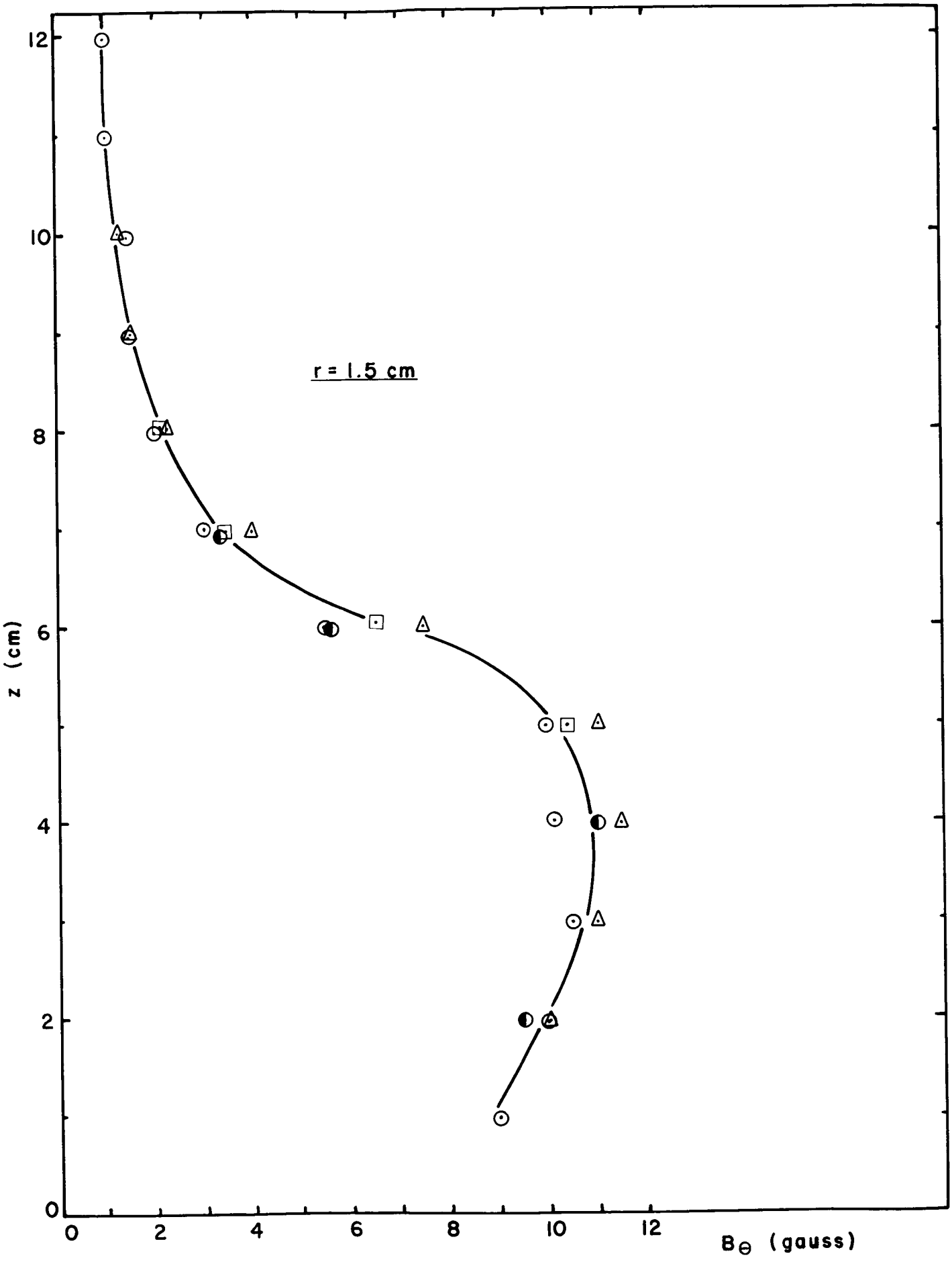

VARIATIONS OF B_e AS A FUNCTION OF Z IN MERCURY FILLED GAP IN THE ABSENCE OF AN APPLIED MAGNETIC FIELD ($B_0 = 0$)

Fig. 4

On the Accuracy of Calculating the Scalar Electrical Conductivity at Very Low Ionization Levels **

by

S. Schweitzer*
University of Pennsylvania
Philadelphia, Pennsylvania

The general validity of mixture rules for calculating the electrical conductivity of a partially ionized plasma has been examined for arbitrary electron-neutral cross-section[1,2] and for a model gas[2,3] having an electron-neutral collision frequency of the form

$$\nu_{en}(g) \propto g^{2m} \qquad (1)$$

where g is the relative electron speed and m is a parameter. Using the third Chapman-Enskog approximation, it is shown[2] that within the uncertainties in the experimental electron-neutral cross-section values Frost's[4] mixture rule for the scalar electrical conductivity offers a satisfactory method of calculation for most engineering applications.

---

* Assistant Professor of Mechanical Engineering, Towne School of Civil and Mechanical Engineering and Institute for Direct Energy Conversion.
Member AIAA.
This work has been partially supported by a NASA Grant NSG-316.

** To be published in the AIAA J.

Frost proposed to calculate the electrical conductivity of a partially ionized gas, using Allis' formula[5] which is only valid in the limit of no ionization. To account for the charged particle interactions, Frost introduces an additional collision frequency inversely proportional to the square of the relative electron speed.

At very low degrees of ionization, one finds[2] that Frost's results may overestimate the electrical conductivity. To augment the investigation of Ref. 2, it is of interest to determine if this is indeed the case. One may argue as follows. Suppose the Lorentzian limit is approached from a partially ionized condition. As the degree of ionization decreases, electron-electron collisions become less frequent and eventually may be regarded as having no effect on the electron velocity distribution function. The electron collision frequency insofar as momentum exchange is concerned may then be considered as the sum of the electron-neutral and electron-ion collision frequencies. The electron-ion collision frequency should then be given by the Rutherford[6] collision cross-section, and Allis' formula should be applicable as a first approximation.

The scalar electrical conductivity has been calculated by using Allis' equation, replacing the electron-neutral collision frequency by $\nu_{en} + \nu_{ei}$ where ν_{en}, the electron-neutral collision frequency, is given by Eq. 1 and ν_{ei} is the Coulomb collision frequency. The electron speed distribution function in Allis' equation is taken to be Maxwellian. This will be justified later. The results are plotted in Figs. 1 and 2 and are compared with those obtained by Frost's formula. The comparison suggests that at low degrees of ionization Frost's method may overestimate the electrical conductivity. The normalizing conductivity is

defined by the mixture rule of Lin, Resler, and Kantrowitz[7]:

$$\frac{1}{\sigma_{add}} = \frac{1}{\sigma_{en}} + \frac{1}{\sigma_{ei}} , \qquad (2)$$

where σ_{en} and σ_{ei} are the Lorentzian and the Spitzer-Härm conductivities respectively, and σ_{en}/σ_{ei} is a measure of the degree of ionization.[2]

For the parameter values of m = -1 and m = 0 (not shown), Frost's method also yields higher conductivity values but the difference is insignificant.

The equivalence between Allis' conductivity (with a Maxwellian distribution function) and Chapman-Cowling's[8] exact result for a Lorentzian gas will now be shown. Allis' conductivity may be written as

$$\sigma = \frac{4\pi e^2}{3 m_e} \int_0^\infty F_e \frac{d}{dg}\left(\frac{g^3}{\nu_{en}}\right) dg = - \frac{4\pi e^2}{3 m_e} \int_0^\infty \frac{dF_e}{dg} \cdot \frac{g^3}{\nu_{en}}\, dg, \qquad (3)$$

where F_e is taken as the normalized Maxwellian distribution function of the electrons, e is the electronic charge, and m_e the mass of the electron.

It is simple to demonstrate that Eq. 3 may be obtained from the closed form expression of the "infinite" Chapman-Enskog approximation to the electrical conductivity of a Lorentzian gas*:

$$\sigma_{en}(\infty) = \frac{e^2}{6\pi n k T} \int f_e^{(0)} \frac{C_e^2}{\phi_{en}^{(1)}}\, d^3 c_e \qquad (4)$$

---

* See Ref. 8, Chapter 10, Section 5.

The quantity n is the gas number density, $f_e^{(0)}$ is the Maxwellian distribution function of the electrons, C_e is the peculiar velocity, c_e is the electron velocity and

$$\phi_{en}^{(1)} = \frac{1}{2\pi} g Q_{en}^{(1)}(g) = \frac{\nu_{en}}{2\pi n_n}$$

where n_n is the number density of the neutral particles. Noting that $F_e = \frac{1}{n_e} f_e^{(0)}$, $n \sim n_n$, $C_e \sim g$, $d^3 c_e = d^3 C_e$, and that

$$f_e^{(0)} = - \frac{kT}{m_e g} \cdot \frac{df_e^{(0)}}{dg}$$

we see that $\sigma = \sigma_{en}(\infty)$. Thus, Allis' equation with a Maxwellian distribution function is identical to the closed form solution in the infinite approximation given by Ref. 8 for a very weakly-ionized gas.

FIGURE CAPTIONS

Figure 1. Normalized Electrical Conductivity as a Function of Ionization for the Electron-Neutral Collision Frequency Model $\nu_{en} \alpha g^2$ $(m = 1)$. The dashed curve represents the third Chapman-Enskog approximation[2].

Figure 2. Normalized Electrical Conductivity as a Function of Ionization for the Electron-Neutral Collision Frequency Model $\nu_{en} \alpha g$ $(m = 1/2)$. The dashed curve represents the third Chapman-Enskog approximation[2].

References

1. Schweitzer, S., "The Tensor Electrical Conductivity of Cesium-Seeded Argon at Atmospheric Pressure," AIAA J. 5, 844-847 (1967).

2. Schweitzer, S., and Mitchner, M., "Electrical Conductivity of Partially Ionized Gases," AIAA J. 4, 1012-1019 (1966).

3. Schweitzer, S., and Mitchner, M., "The Electrical Conductivity of a Partially Ionized Gas in a Magnetic Field," Proceedings of the 7th Symposium on Engineering Aspects of MHD, Princeton University, March 1966. Complete version published as Phys. Fluids, 10, 799-806 (1967).

4. Frost, L. S., "Conductivity of Seeded Atmospheric Pressure Plasmas," J. Appl. Phys. 32, 2029-2039 (1961).

5. Allis, W. P., Handbuch der Physik (Springer-Verlag, Berlin, 1956), Vol. XXI, p. 413.

6. Rose, J. J., and Clark, M., Plasma and Controlled Fusion (The MIT Press and John Wiley and Sons, N. Y., 1961).

7. Lin, S. C., Resler, E. L., and Kantrowitz, A., "Electrical Conductivity of Highly Ionized Argon," J. Appl. Phys. 26, 95-109 (1955).

8. Chapman, S., and Cowling, T. G., The Mathematical Theory of Non-Uniform Gases (Cambridge University Press, London, 1952).

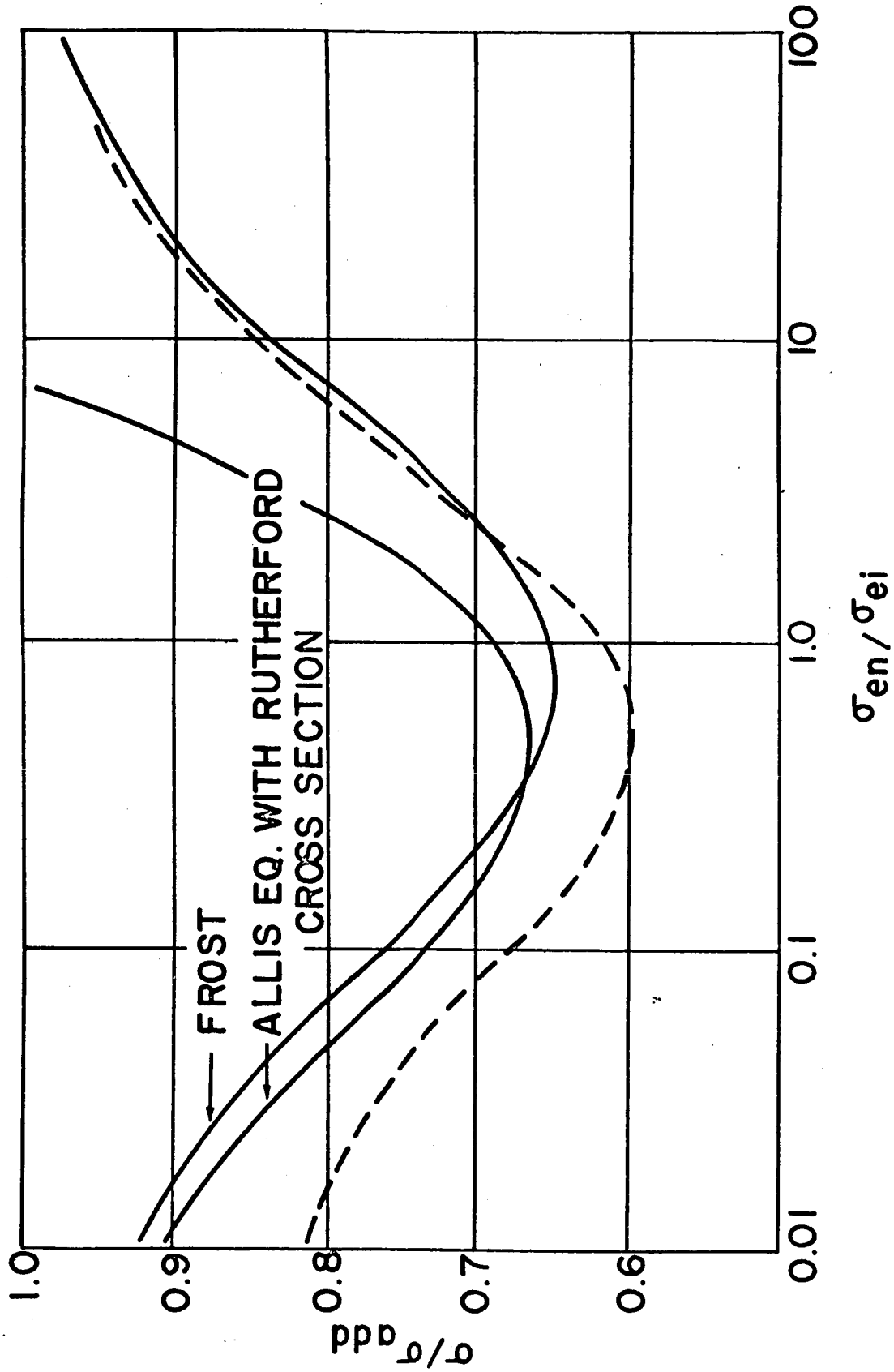
1.0
0.9
0.8
0.7
0.6
q/q_add
0.01
0.1
1.0
10
100
σ_en / σ_ei
FROST
ALLIS EQ. WITH RUTHERFORD CROSS SECTION

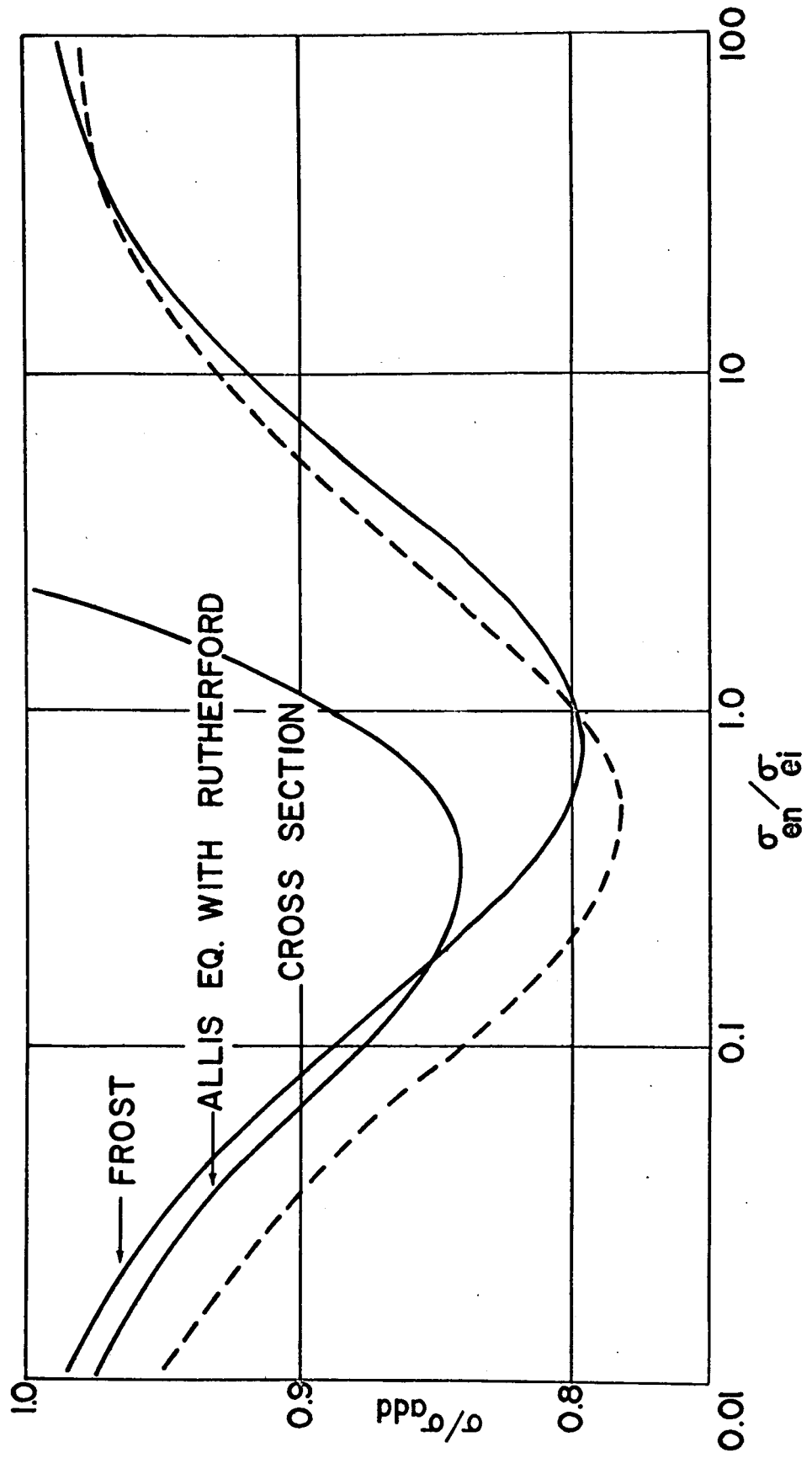
1.0
0.9
0.8
σ/σ_ddd
100
10
1.0
0.1
0.01
σ_en/σ_ei
FROST
ALLIS EQ. WITH RUTHERFORD
CROSS SECTION

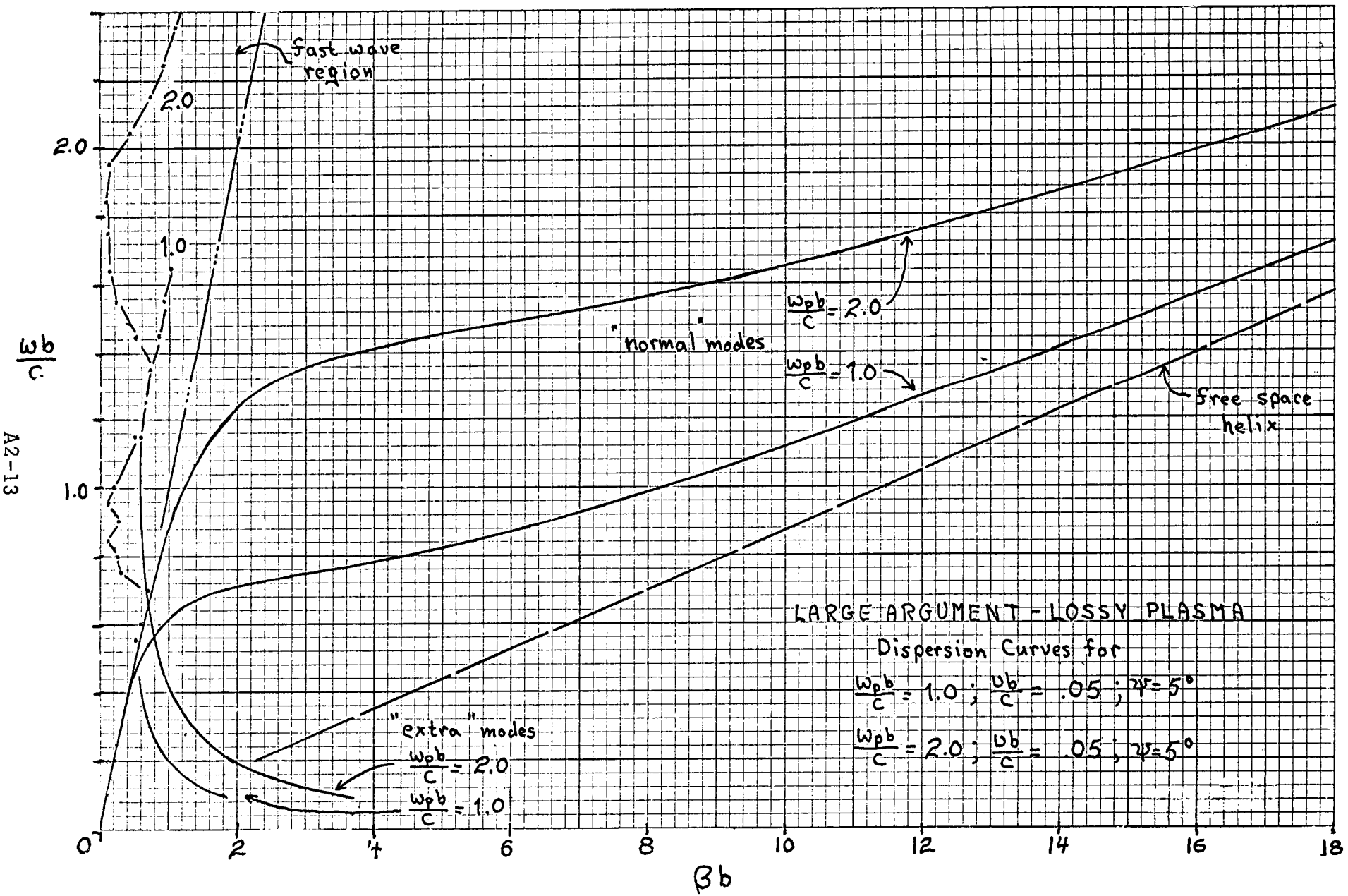
fast wave region
2.0
1.0
"normal" modes
$\frac{\omega_{pb}}{c} = 2.0$
$\frac{\omega_{pb}}{c} = 1.0$
free space helix
"extra" modes
$\frac{\omega_{pb}}{c} = 2.0$
$\frac{\omega_{pb}}{c} = 1.0$
LARGE ARGUMENT - LOSSY PLASMA
Dispersion Curves for
$\frac{\omega_{pb}}{c} = 1.0$; $\frac{v_b}{c} = .05$; $\psi = 5°$
$\frac{\omega_{pb}}{c} = 2.0$; $\frac{v_b}{c} = .05$; $\psi = 5°$
$\frac{\omega b}{c}$
βb
0
2
4
6
8
10
12
14
16
18
2.0
1.0

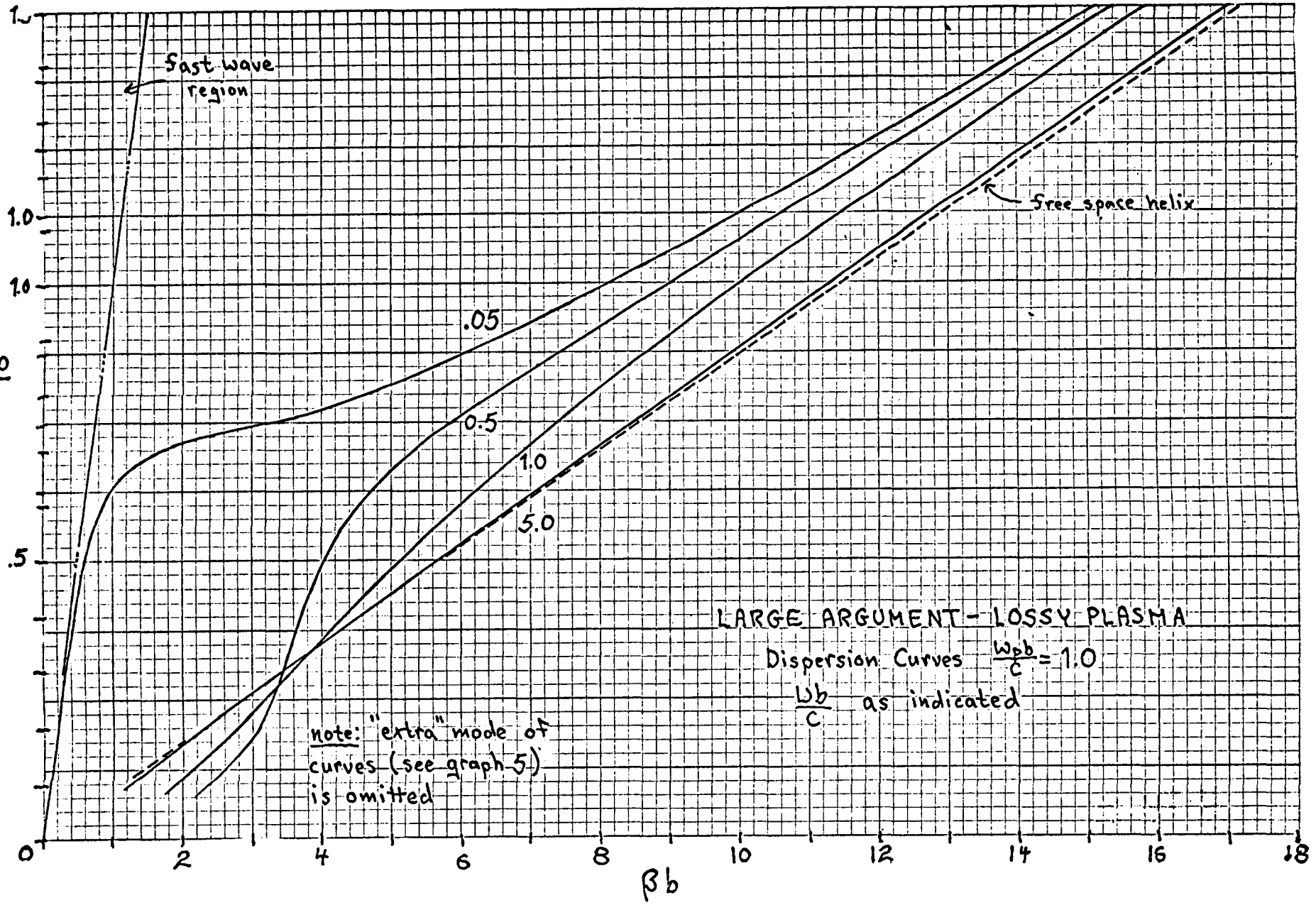
fast wave region
free space helix
.05
0.5
1.0
5.0
LARGE ARGUMENT - LOSSY PLASMA
Dispersion Curves $\frac{\omega_p b}{c} = 1.0$
$\frac{\omega b}{c}$ as indicated
note: "extra" mode of curves (see graph 5) is omitted
$\frac{\omega b}{c}$
βb
0
.5
1.0
1.0
1.~
2
4
6
8
10
12
14
16
18

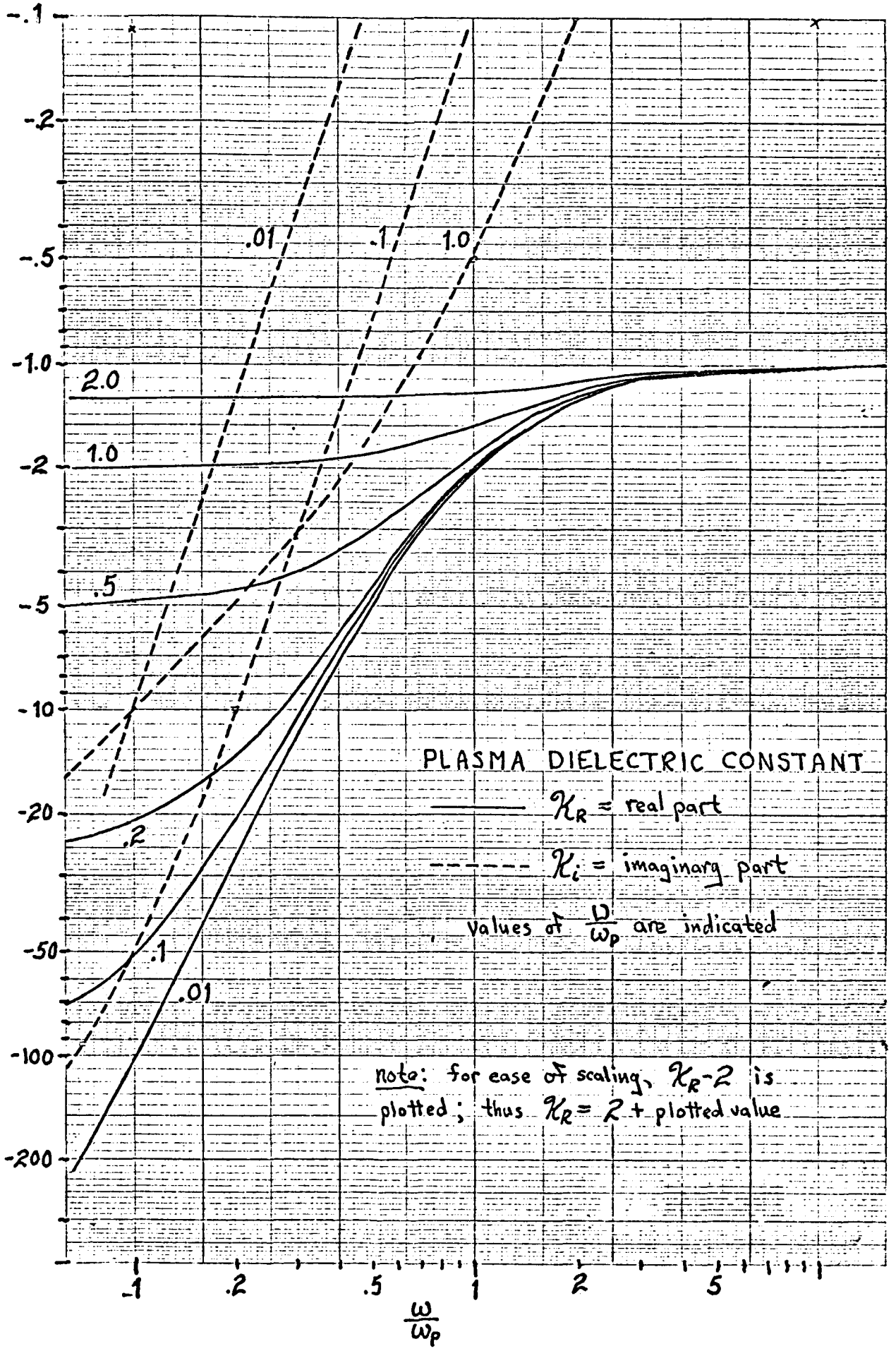
-.1
-.2
-.5
-1.0
-2
-5
-10
-20
-50
-100
-200
.01
.1
1.0
2.0
1.0
.5
.2
.1
.01
PLASMA DIELECTRIC CONSTANT
$\mathcal{K}_R$ = real part
$\mathcal{K}_i$ = imaginary part
values of $\frac{\omega}{\omega_p}$ are indicated
note: for ease of scaling, $\mathcal{K}_R - 2$ is plotted; thus $\mathcal{K}_R = 2 +$ plotted value
.1
.2
.5
1
2
5
$\frac{\omega}{\omega_p}$

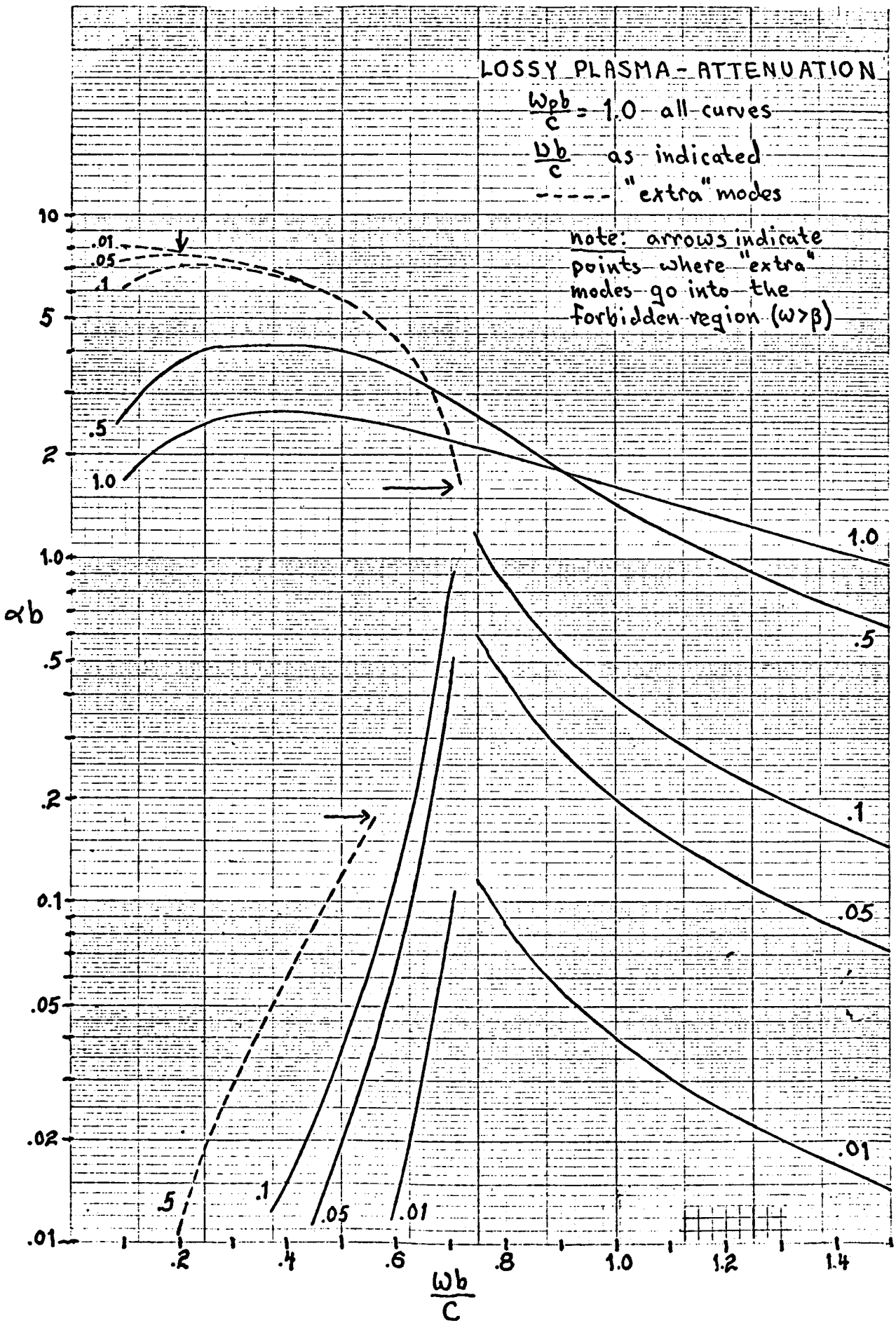
LOSSY PLASMA - ATTENUATION
$\frac{\omega_{pb}}{c}$ = 1.0 - all curves
$\frac{\nu b}{c}$ as indicated
----- "extra" modes
note: arrows indicate points where "extra" modes go into the forbidden region ($\omega > \beta$)
αb
$\frac{\omega b}{c}$
10
5
2
1.0
.5
.2
0.1
.05
.02
.01
.2
.4
.6
.8
1.0
1.2
1.4
.01
.05
.1
.5
1.0
.5
.1
.05
.01
.5
.1
.05
.01

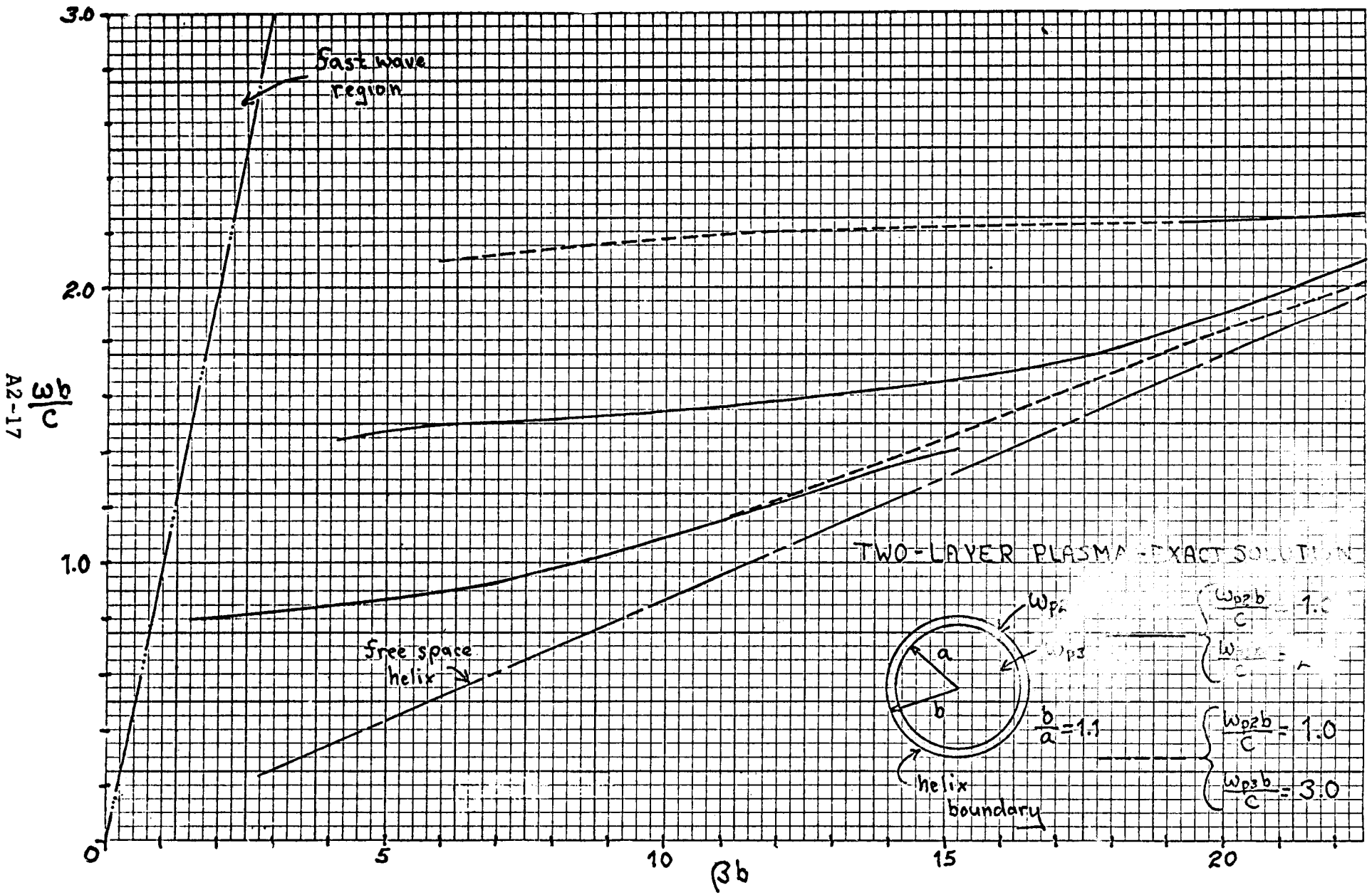
3.0
2.0
1.0
0
ω/c
A2-17
Fast wave region
Free space helix
5
10
15
20
βb
TWO-LAYER PLASMA - EXACT SOLUTION
ω_p2
ω_p3
a
b
b/a = 1.1
helix boundary
ω_p2 b / c = 1.0
ω_p3 b / c = 3.0

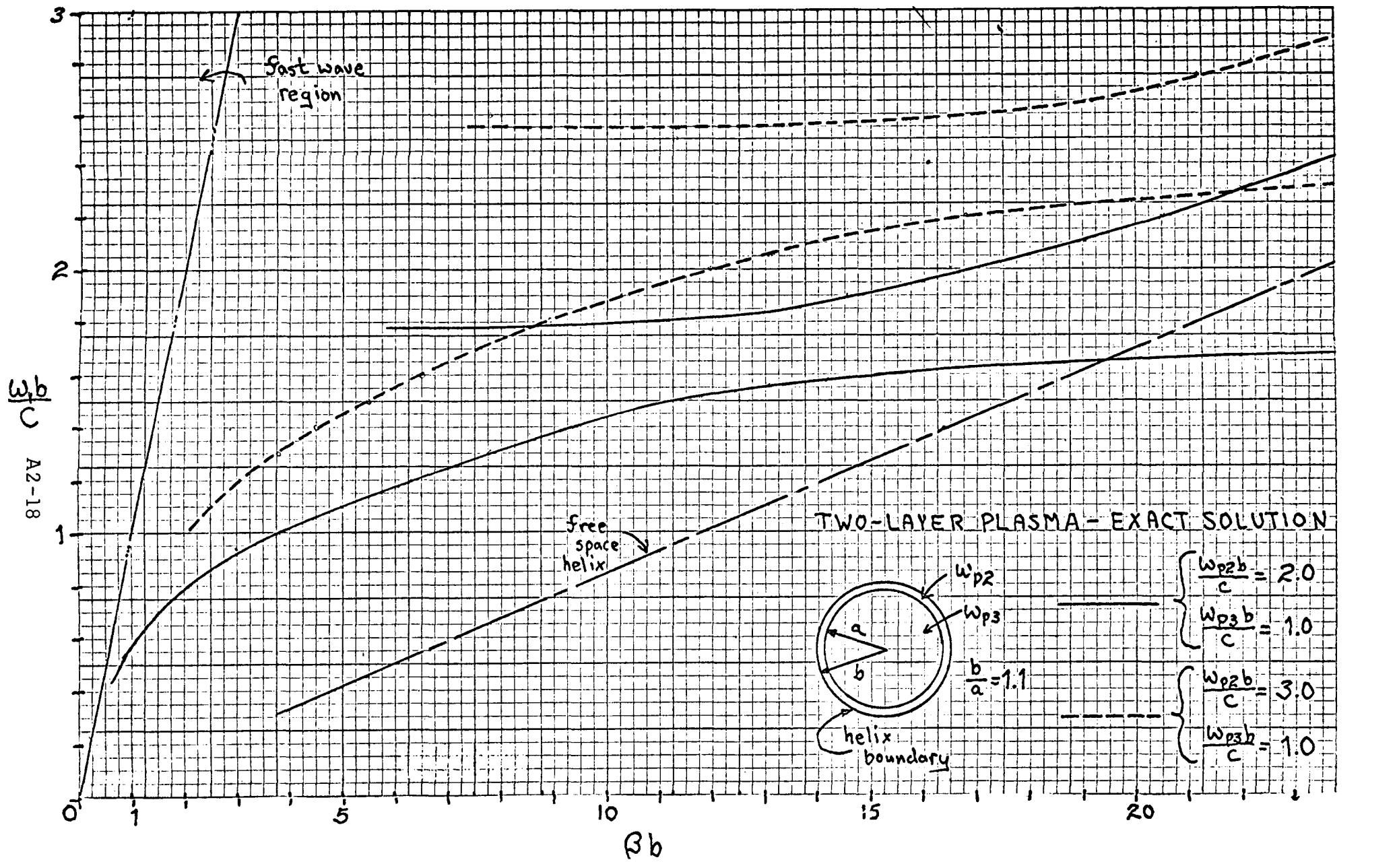
3
2
1
0
1
5
10
15
20
ωb/c
βb
fast wave region
free space helix
TWO-LAYER PLASMA - EXACT SOLUTION
ωp2
ωp3
a
b
b/a = 1.1
helix boundary
ωp2b/c = 2.0
ωp3b/c = 1.0
ωp2b/c = 3.0
ωp3b/c = 1.0

ELECTROCHEMICAL ENGINEERING

APPENDIX

A-3

Freezing Potentials

Senior Investigator: Dr. L. Nanis
Graduate Student: Irving Klein

The background for the present research lies in the work done by Workman and Reynolds[1] in the late 1940's regarding the static electrification of thunderclouds. However, since their pioneering effort, no significant publication has appeared on the subject. They correctly observed the "freezing potential" to be a voltage that is generated when an ionic solution is frozen between two electrodes. If one electrode is used as a reference and the other as a cold finger, the potential first appears when the first layer of ice is formed on the cold finger. The aspect that immediately distinguishes this potential from other electrochemical phenomena is its magnitude, which has been observed to exceed 100 volts. It is a transient phenomenon that rises and then decays as the freezing ionic solution undergoes complete solidification.

The resulting potential is hypothesized to be caused by the selective trapping of an ionic species in the ice lattice. This separation of charge destroys the electrical equilibrium in the solution, and a voltage is generated. The present research included a series of calculations that verify that the seat of the potential is indeed in the ice and not in the electrical double layer immediately adjacent to the ice interface and that, therefore, the ice is being utilized in a manner analogous to the dielectric in a capacitor. It should be noted that because of the small capacitance inherent in the ice, only a small ionic imbalance is necessary to produce the large observed voltages. It has been calculated, within an order of magnitude, that an excess ion count of $100/cm^2$ is enough to produce potentials as high as 100v.

Note that implicit in this result lies the basis for postulating that the "freezing potential" is a phenomenon that takes place on a scale small enough to exhibit statistical randomness. This effect considerably negates any attempts to obtain extreme precision in the experimental data and offers an explanation for the considerable irreproducibility sometimes as high as 75%, in the data.

---

[1] E. J. Workman & S. E. Reynolds, Physical Review, Vol. 78, No. 3, p. 254, 1950

The "freezing potential" was experimentally found to be influenced by the following parameters: 1) the type of ionic species dissolved in the solution; 2) the amount or concentration of the dissolved ions; 3) the chemical composition of the cold finger electrode upon which freezing takes place. The first two parameters were studied in great depth by Workman and Reynolds[1], and were thus checked by duplicating a small portion of their results; but the present research primarily concentrated in examining the importance of the freezing substrate, which until now has been unexplored.

A rigorous investigation left no doubt that the composition of the freezing substrate had a significant effect in influencing the magnitude of the potential developed in identical experimental solutions. The next logical step was to determine what properties inherent to the substrate could produce the observed effects.

Ostensibly it was first thought that the potential of zero charge of the metal constituting the freezing surface[2] was the dominant factor to consider. This potential of zero charge corresponds to a net charge distribution of zero at the surface of the metal, and serves as the zero point on the rational potential scale for the particular metal being studied. It was, therefore, hypothesized that a positive rational potential prior to freezing, i.e. a lack of electrons, would intensify a negative "freezing potential" and interfere with a positive one; whereas a negative rational potential prior to freezing would have an opposite effect. Within the limits of the experimental uncertainty, however, this PZC effect turned out to be of negligible importance.

What was shown to be important, however, was the thermal diffusivity of the metal. The thermal diffusivity affects the rate at which

---

[2] Three-quarter progress report (10/1/64 - 6/30/65) of the Univ. of Penn. Electrochemistry Laboratory, Studies in the Fundamental Chemistry of the Fuel Cell Reactions, pp. AI-36 to AI-41, Contract NSG-325.

the ionic solution freezes and thereby controls charge separation. That is to say, extremely rapid freezing and extremely slow freezing tend to reduce the magnitude of the potential and some optimum rate corresponding to a maximum voltage can be obtained.

Another important characteristic of the freezing substrate was found to be its chemical composition. This was dramatically shown in two series of experiments.

The first experiment consisted of freezing identical ionic solutions on two different substrates, one was a sheet of silver and the other consisted of this same silver sheet, but plated with a thin layer of silver-silver chloride. The freezing time for a given solution on these two substrates is identical; therefore, the observed differences in the "freezing potentials" could only be generated by some sort of chemical effect. The silver-silver chloride substrate consistently yielded higher absolute potential values than the silver one, regardless of the solutions employed, i.e., regardless of their tendency to produce either positive or negative "freezing potentials".

The second, and perhaps more dramatic series of experiments utilized mercury as the freezing surface. By impressing a potential on the mercury surface, one was able to control its polarity prior to freezing. When the mercury was made cathodic, potentials as high as 40v were observed upon freezing dilute solutions of ammonium chloride, but as soon as the mercury was made anodic no significant "freezing potential" was detected. In explaining this phenomenon, it is hypothesized that the anodic condition created an oxide layer on the mercury surface and thereby altered its chemical characteristics. The results of this series of experiments are shown in Fig. (1), where the abscissa corresponds to the initial rational potential, i.e. the potential of the substrate on the rational scale prior to the initiation of freezing the solution, and the ordinate corresponds to the "freezing rational potential".

This is as far as the study has been pursued, and as yet no theoretical correlation that fully explains the effects of the chemical composition of the surface on the "freezing potential" has been proposed. However, it appears as if there must be some sort of chemical bonding present that helps to either promote or negate charge separation as the ice begins its selective entrapment. In order to investigate more thoroughly the dependence of the "freezing potential" on the surface composition, a recommendation for future research would involve the utilization of platinum as a freezing substrate, and the surface chemical composition of this metal could then be accurately controlled by electrolytic means.

As one final aspect of this investigation, the possibility of utilizing the "freezing potential" or some related phenomenon involving charge separation as a source of electrical power must be considered. Although this research presents no results regarding the currents developed during the freezing process, the experimental work of Workman and Reynolds, as well as present theoretical calculations, indicate that a charge separation corresponding to one microcoulomb/cm^3 of ice frozen is a good approximation. Therefore, the power produced is indeed small if one considers that it takes about one minute to optimally freeze one cm^3 of ice, and the power produced is on the order of 10^{-6} watts/cm^3 of solution frozen.

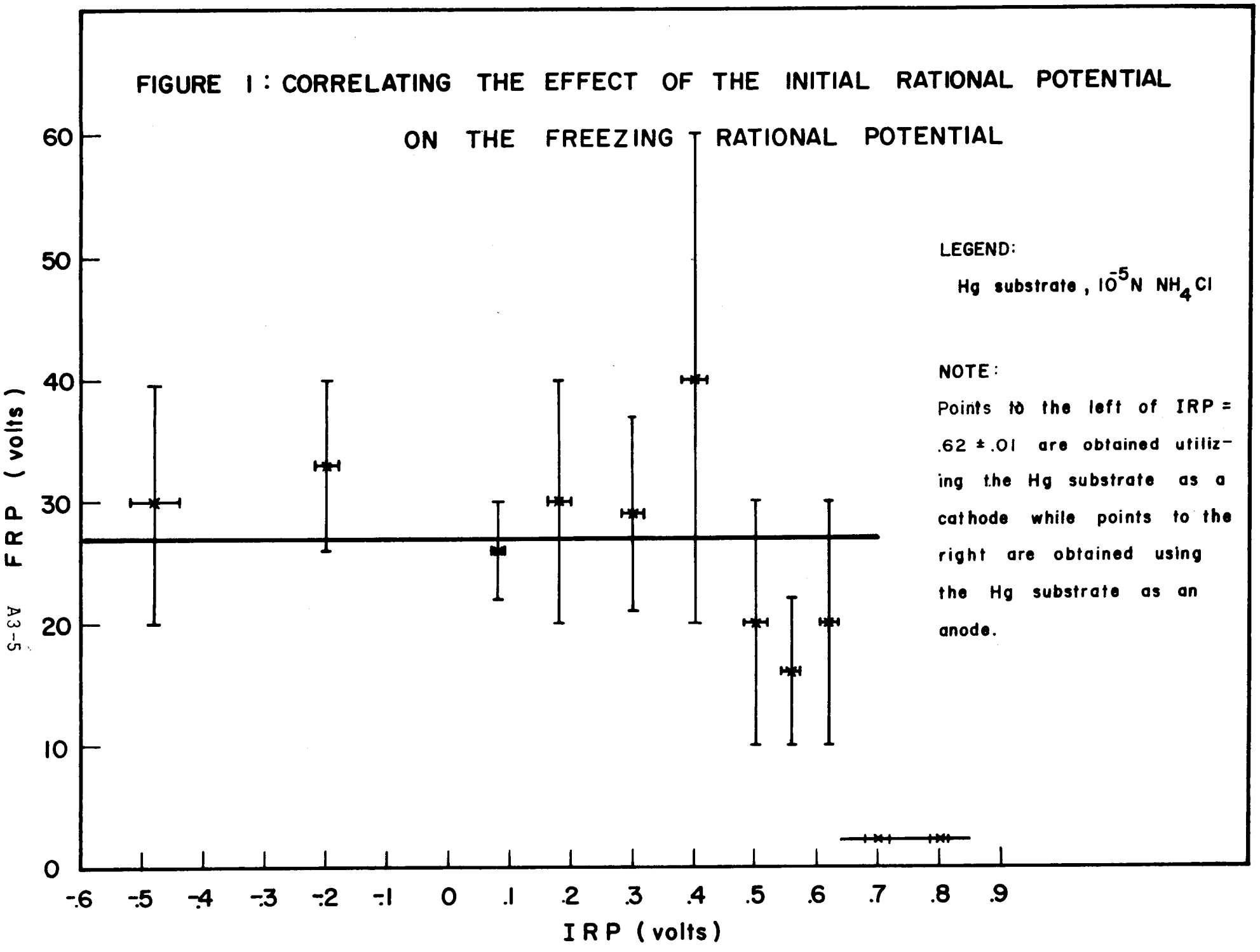
FIGURE 1 : CORRELATING THE EFFECT OF THE INITIAL RATIONAL POTENTIAL ON THE FREEZING RATIONAL POTENTIAL
LEGEND:
Hg substrate , 10^{-5}N NH_4Cl
NOTE:
Points to the left of IRP = .62 ± .01 are obtained utilizing the Hg substrate as a cathode while points to the right are obtained using the Hg substrate as an anode.
FRP (volts)
IRP (volts)
60
50
40
30
20
10
0
-.6
-.5
-.4
-.3
-.2
-.1
0
.1
.2
.3
.4
.5
.6
.7
.8
.9

Current and Potential Distribution in Cylindrical Geometries: Engineering Application to Fuel Cell Design

Senior Investigator: Dr. L. Nanis

Graduate Student: Wallace Kesselman

By a procedure identical to that reported last quarter, solution of the Laplace equation in cylindrical coordinater,

$$\frac{\partial^2\theta}{\partial r^2} + \frac{1}{r}\frac{\partial\theta}{\partial r} + \frac{\partial^2\theta}{\partial z^2} = 0 \qquad (1)$$

by means of Fourier-Bessel (Hankel) transforms yields as a solution for the potential at the disk

$$V(r) = \int_0^\infty A(p) J_0(pr)\, dp \qquad (2)$$

and also for the radial variation of current density

$$J(r) = -k \int_0^\infty p A(p) J_0(pr)\, dp \qquad (3)$$

Here, J_0 represents the Bessel function of the first kind and zero order.

We wish to take into account the effects of overpotential; hence, this consideration must enter into our boundary conditions. Combining the linear current-overpotential relationship,

$$J = -k\frac{\partial V}{\partial z} = J_0 \frac{zF}{RT}\eta \; ; \qquad r < a \qquad (4)$$

with the condition that

$$J = -k\frac{\partial V}{\partial z} = 0 \qquad r > a \qquad (5)$$

and also that

$$V_0 = \text{constant} = V(r) + \eta(r) \qquad r < a \qquad (6)$$

the result is obtained that

$$V_0 = \int_0^\infty A(p) J_0(pr)\, dp + c\int_0^\infty p\, A(p) J_0(pr)\, dp \qquad r < a \qquad (7)$$

$$0 = \int_0^\infty p\, A(p) \mathcal{J}_0(pr)\, dp \qquad r > a \tag{8}$$

where $$c = \frac{kRT}{J_0 zF} \tag{9}$$

Equations (7)-(9) can now be solved, in principle at least, for A(p) which, when substituted into (2) and (3), will then give V(r) and J(r), the potential and current distribution.

Solution of (7) and (8) amounts to the solution of the dual integral equation, which has already been treated by Busbridge[1]. Application of this approach reduces the problem to the solution of a singular Fredholm integral equation:

$$A(x) = \frac{2aV_0}{\pi}\,\frac{\sin x}{x} - \frac{2c}{a\pi}\cos x \int_0^\infty \sin p\, A(p)\, dp$$

$$-\frac{2c}{a\pi}\, x \cos x \int_0^\infty \frac{A(p)\sin p}{p^2-1}\, dp$$

$$+\frac{2c}{a\pi}\, x \sin x \int_0^\infty \frac{p\, A(p)\cos p}{p^2-1}\, dp \tag{10}$$

This integral equation has a degenerate kernel, which is amenable to analytic solution. The theory is rather straightforward[2] for linear equations of the non-singular type, but in the present case problems of convergence are being encountered, which are now being investigated in the light of the principles of summability of integrals and Cauchy principle values. The results will be reported in the next quarter.

REFERENCES

(1) Busbridge, Proc. London Math. Soc., 44 (2), 115 (1938)

(2) Hildebrand, Methods of Applied Mathematics, Prentice Hall (1961) p. 406

Foaming Electrolyte Fuel Cell

Senior Investigator: Dr. L. Nanis
Research Specialist: A. P. Saunders

The previous report stated that immersion of platinum electrodes in a foam structured electrolyte gave improved cell performance when compared with platinum electrodes immersed in normal electrolyte with the fuel gas bubbling freely around it. In the previous study, there was possibly a degree of depolarization (in the non-foamed condition) due to interchange of electrolyte between the respective electrode compartments.

In order that a more accurate comparison of the two systems may be obtained, i.e., foam and non-foamed, a series of experiments was performed to determine the maximum diffusion limiting current which may be sustained at various KOH concentrations. The first investigation was made on bright platinum mesh electrodes immersed in 2N KOH with the fuel gas bubbling rapidly and freely stirring the electrolyte. The cell previously reported was modified as shown in Fig. 1., to hold approximately 300 ml in each electrode compartment. "D" porosity glass frits were used to separate the respective electrode chambers, and a fine ceramic frit (approx. 5 micron pore diam.) was used at the gas inlets. This provides a finely dispersed gas flow with good gas saturation of the electrolyte.

Non-reproducible H_2 electrode overpotential effects made it difficult to obtain meaningful potential-current curves useful for comparison purposes. Any change in load could not be reversed back to the same potential-current relationship. It was also found that an apparent-maximum electrode activity could be produced by using an external power supply and by raising the H_2 electrode potential above 0.8 volts (vs H_2 ref). To assist in obtaining useful data, it was decided to record the potential changes while passing a constant current, based on the assumption that an increase in efficiency using a foam structure may be easily identified by the increased time required for the potential to rise to an arbitrarily fixed point. The circuit employed to pass the fixed current is shown in Fig. 2. Potential changes were recorded on a Varian G22A recorder.

The first and subsequent experiments disclosed what is believed to be a hitherto unreported phenomenon. When the anode H_2 potential rises to approximately 0.3 volts, the small oscillations of the potential (due in part to the stirring action of the bubbling gas) begin to increase in amplitude, and when the potential reaches 0.5 to 0.6 volts a definite behavior pattern is clearly discernible. Immediately after a peak in potential, a rejuvenation of the electrode activity occurs. This reactivation does not last very long, with the mean potential rising to the value it recently vacated, and continuing to rise until another peak repeats the reactivation cycle. At or around +0.7 volts, the cyclic potential excursions are large and continue until the electrode potential does not return from a peak but continues up to 1.6 volts as though a critical threshold has been exceeded. On removing the external power supply and placing the cell on open circuit, the H_2 electrode potential declines slowly to the 0.7 volts region whereupon it quickly drops to the normal open circuit H_2 potential (0.002 volts). The cyclic potential effects mentioned above appear to be controlled primarily by the potential level and are virtually independent of current magnitude. The time required to attain a potential region does vary according to the current in a manner suggesting coulombic effects.

The time taken for an electrode potential to rise above 0.8 volts at a given current varies as does the amount of reactivation cycles which occur. The cyclic potential swings have not been thoroughly analyzed; however, at first glance there does not seem to be any true periodicity. An illustration of the reactivation cycles is given in Fig. 3 which shows that one electrode entered the oxygen region (1.6 volts) after 15 minutes while the identical conditions produced the same effect in 19 minutes in a subsequent experiment.

The two potential traces are copied from the recorder chart, and although they do not exactly portray the individual peaks, they do give an accurate overall picture of how the reactivation cycles occur.

The behavior of the O_2 electrode has not been dwelt upon here as it behaves very reproducibly, the potential uniformly falling between 0.73 and 1 volt at maximum currents, when its area is equal to or greater than that of the H_2 electrode.

It is believed that the reactivation phenomenon is due to unequal current distribution and overpotential on the electrode, the platinum mesh electrode being especially conducive to this with its many points and edges. Passivated areas of the electrode are forced, under the impetus of the driving potential from the external power supply, to pass current by an alternative reaction to the oxidation of Hydrogen, causing reactivation of that, and possibly adjacent areas, possibly by oxide formation. It is interesting to note that if an electrode with large oxygen overpotential is left on open circuit for several minutes, large overpotential remains when current is again passed. If, however, the electrodes are externally shorted to each other, a certain amount of reactivation occurs. The increase in amplitude of the oscillations seen above 0.3 volts is also taken as an indication that this process may be in effect even at this low mean potential, apart from fluctuations due to the stirred electrolyte.

Further work is being done along the lines of varying the electrode geometry to establish any relationship to the cyclic phenomena.

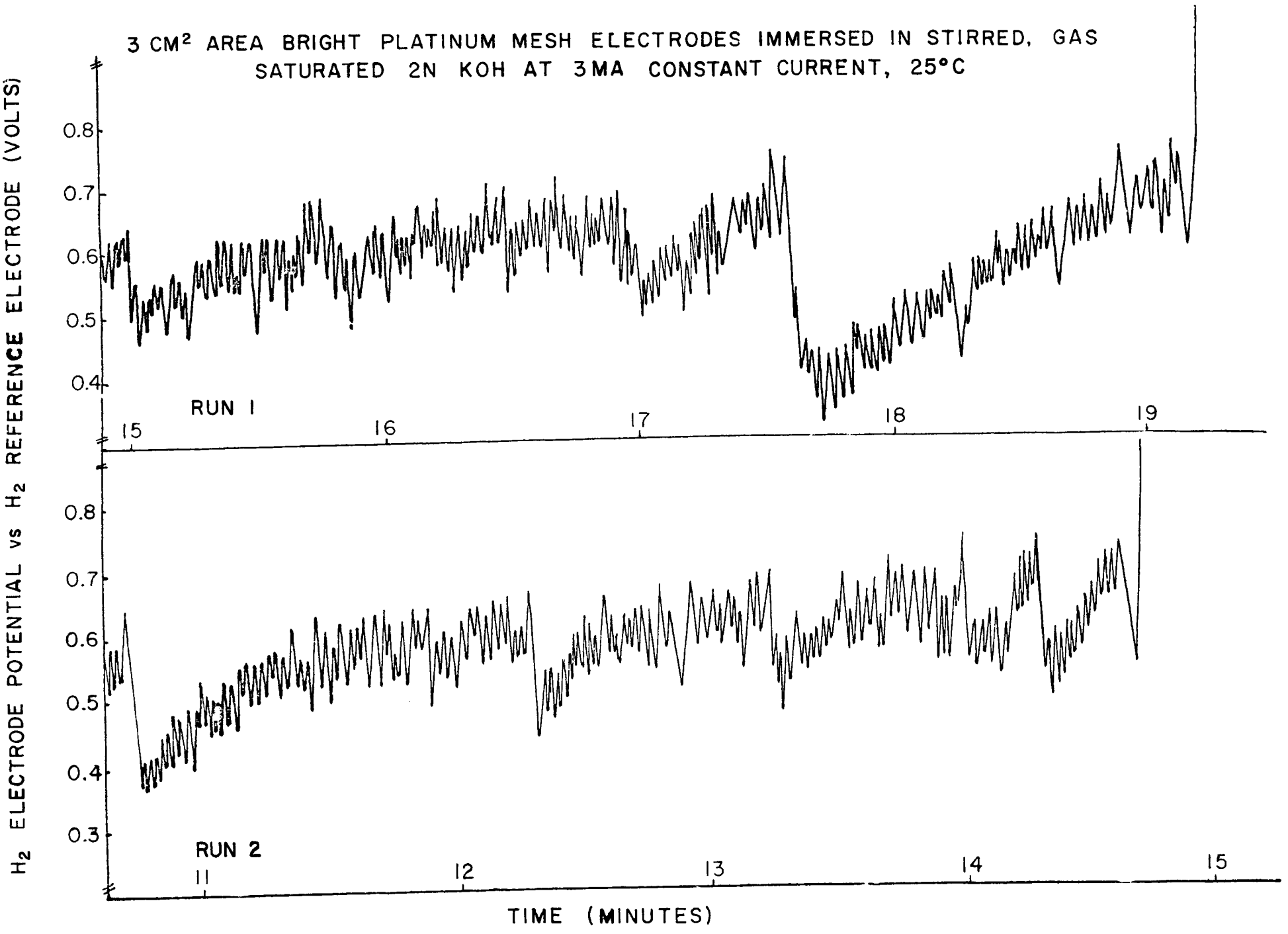

REACTIVATING CYCLIC INSTABILITY

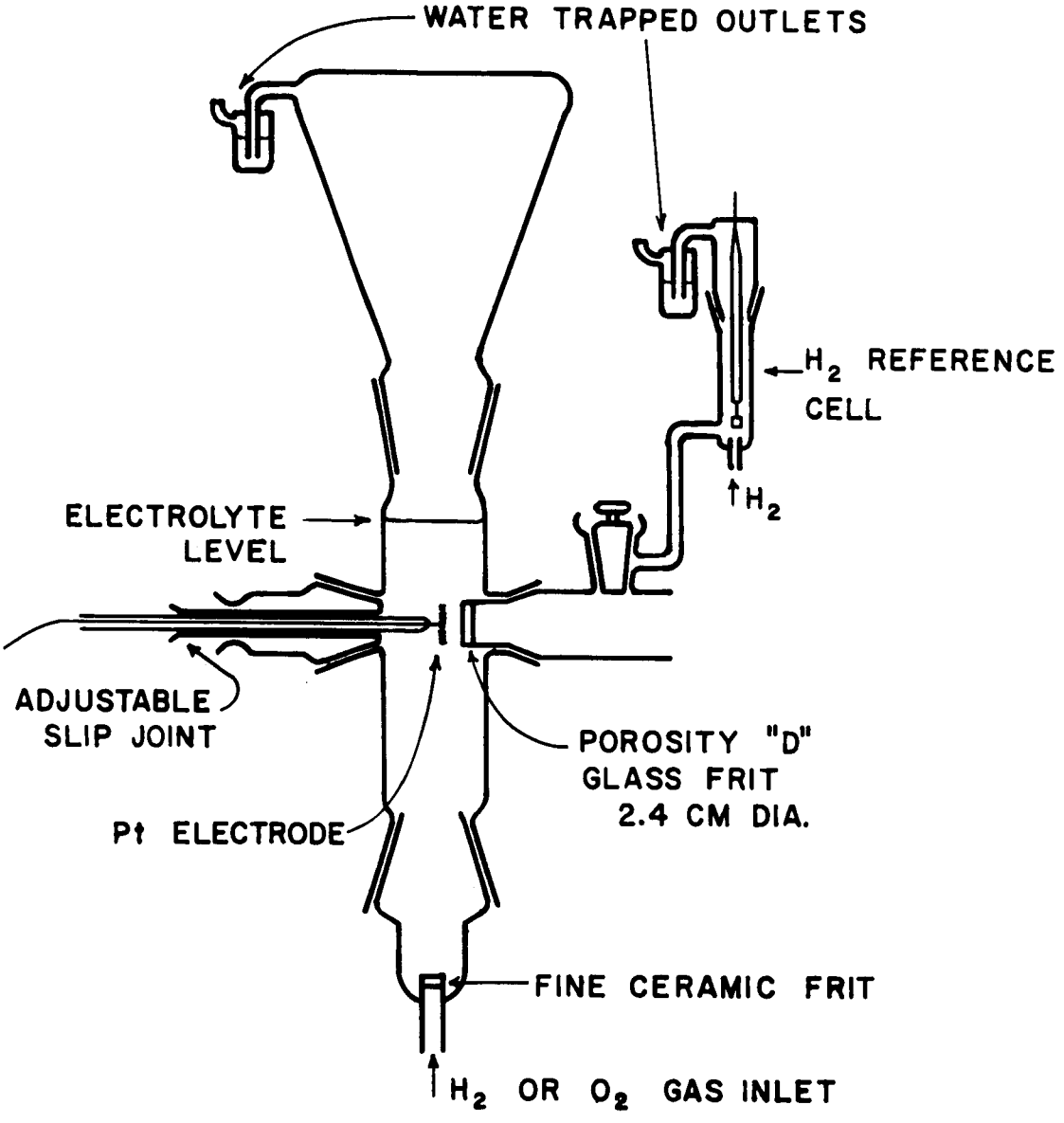
WATER TRAPPED OUTLETS
H_2 REFERENCE CELL
H_2
ELECTROLYTE LEVEL
ADJUSTABLE SLIP JOINT
POROSITY "D" GLASS FRIT 2.4 CM DIA.
Pt ELECTRODE
FINE CERAMIC FRIT
H_2 OR O_2 GAS INLET

Fig. 1

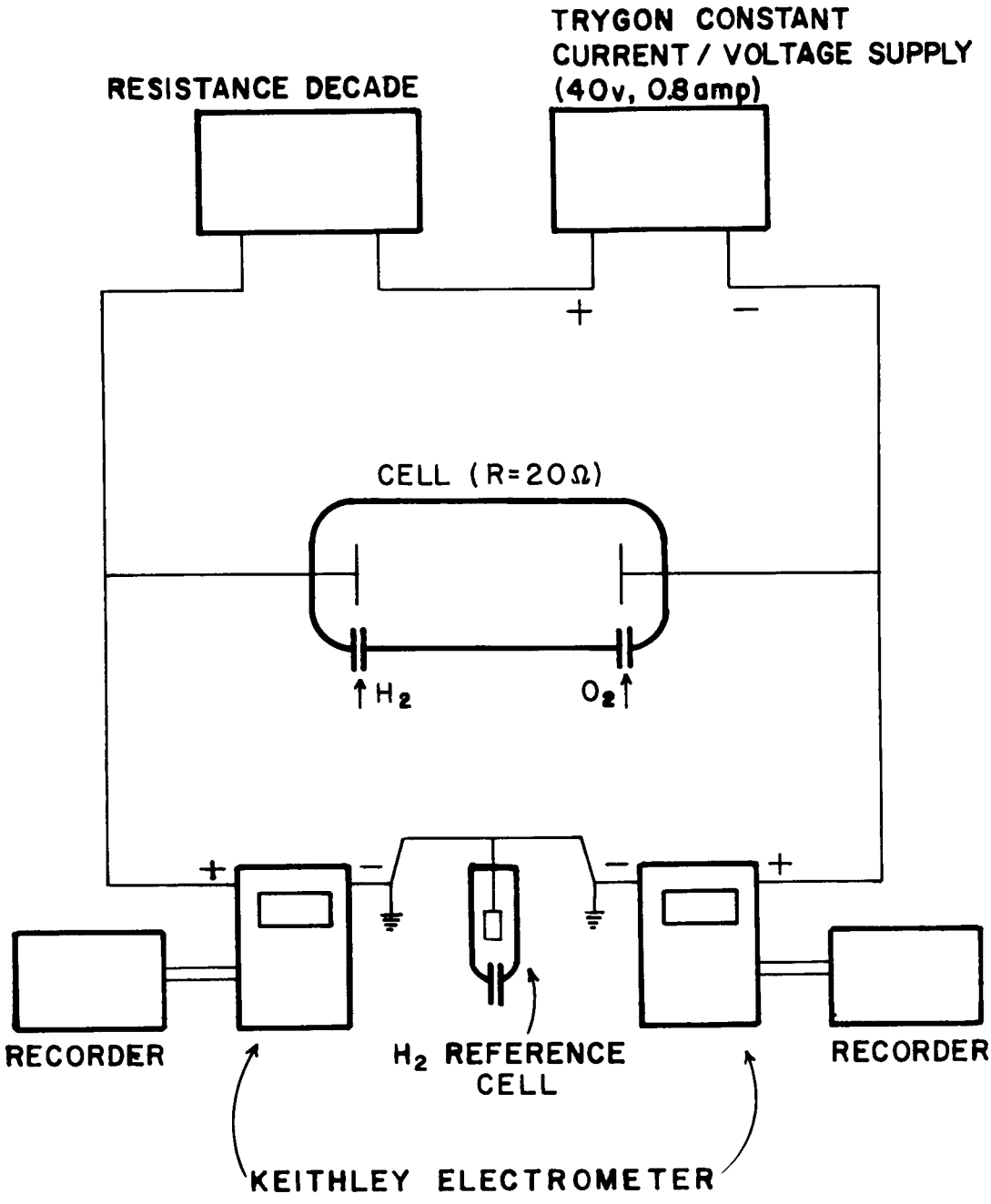

SCHEMATIC PRESENTATION OF CONSTANT CURRENT SUPPLY AND CIRCUIT USED IN OBTAINING REACTIVATION CYCLING

Fig. 2

Atomic Scale Electrode Processes

P. Javet L. Nanis

As previously discussed in INDEC-SR-9, platinum is of great electrochemical interest. There are, however, difficulties linked with the use of this metal in the F.I.M.. Among the principal difficulties encountered in our study are

1) The voltage at which the image has maximum resolution is very close to the field evaporation voltage leading to non-stable images.

2) The surface is very sensitive to contamination with residual gases.

3) Good resolution can be obtained only at liquid hydrogen temperature. These three points have proven very difficult to overcome. Even for the best conditions (low voltage, where control is easier, small tip diameter, for which the temperature requirement is less drastic, and cooling down to solid nitrogen temperature), the resolution for Pt has been insufficient (~ 10 Å). Between tungsten and platinum, however, four metals could be considered, namely Ta, Ir, Re, and Nb[1]. The classification is made on the basis of the field needed for the evaporation of a metallic atom. The values in MV cm^{-1} are: W: 1068-804 (depending on the orientation considered); Ta: 893; Ir: 886; Re: 851; Nb: 801; Pt: 786. The most interesting of the suitable metals is certainly Ir, whose properties are very close to Pt, and which has been the object of many recent electrochemical studies.

We have prepared successfully good Iridium tips and have obtained fairly good resolution (currently 9 Å and, in some cases, 6.5 Å). Iridium is well suited for our investigation. Preliminary measurements

on these Ir tips have shown that only a few layers (2 to 3) of an atomically smooth surface are perturbed by bringing the tip to atmospheric pressure. A particular hypothesis due to Schuldiner[2] concerning dermasorption of oxygen (penetration of oxygen into the lattice) will be checked with this method. The surface states of oxygen electrosorbed on Iridium may be correlated with effectiveness of this material as a fuel cell anode.

References

(1) E. W. Müller, "Advances in Electronics and Electron Physics" 13, 83 (1960) Academic Press, New York.

(2) S. Schuldiner, T. B. Warner, J. Electrochem. Soc. 112, 212 (1965).

Decay of Activation Overpotential for Potential Dependent Capacitance

P. Javet L. Nanis

Abstract

The use of a general polynomial expression for electrode-electrolyte capacitance as a function of electrode potential permits evaluation of the corresponding decay of potential with time following current interruption. A well-known result due to Frumkin is obtained as a special limiting case. Application to experimental problems is made.

****

The effect of potential dependent electrode-electrolyte interfacial capacitance ($C = f(\eta)$) has been treated recently[1] for galvanostatic transients. The mathematical treatment of the build-up of activation overpotential with time was aided by representation of the C, η relation in the form of a polynomial series as

$$C(\eta) = C_o + C_1\eta + C_2\eta^2 + \ldots \qquad \text{Eqn. 3.5-1}$$

Although theoretically derived forms are much more complex[2][3], the series of Eqn. 3.5-1 is a preferred form for fitting experimental data.

In the same way as for charging, the capacitive current, J_C, during decay following open circuit condition and the Faradaic current are given by the relations

$$J_C = C\frac{\partial \eta}{\partial t} \qquad \text{Eqn. 3.5-2}$$

$$J_F = J_0\left[\exp\left(\frac{-\alpha z \mathcal{F}\eta}{RT}\right) - \exp\left(\frac{(1-\alpha)z\mathcal{F}\eta}{RT}\right)\right] \qquad \text{Eqn. 3.5-3}$$

For the case of total current, J_T, equal to zero,

$$J_T = J_F + J_C = 0 \qquad \text{Eqn. 3.5-4}$$

For decay, the differential equation obtained from Eqns. 3.5-2, 3.5-3, 3.5-4 can be integrated only for special values of α ($\alpha = 0$, 0.5, 1.0) when the capacitance, C, is constant. If the limiting case of linear approximation to Eqn. 3.5-3 is permissible, generally for small steady state overpotential, η_o, the decay following interruption at t = 0 may be readily computed using the potential-capacitance relation suggested in Eqn. 3.5-1. The result is

$$t = \frac{RT}{z\mathcal{F}J_0}\left[C_0 \ln\frac{\eta_o}{\eta} - C_1(\eta-\eta_o) - \frac{C_2}{2}(\eta^2-\eta_o^2)\right.$$

$$\left. - \frac{C_3}{3}(\eta^3-\eta_o^3) - \cdots\right] \qquad \text{Eqn. 3.5-5}$$

This result is limited to a small potential region where extensive variation of capacitance might not be expected.

For steady state overpotential (before current interruption), in which the first term only of Eqn. 3.5-3 (Tafel region) predominates, the condition $\eta = \eta_o$ at $t = 0$ in combination with Eqns. 3.5-1, 3.5-2, 3.5-3, 3.5-4 permits ready evaluation of the potential as a function of time following current interruption. The result is

$$t = \frac{b}{\alpha J_o}\left[C_0(e^{\eta/b} - e^{\eta_o/b}) + C_1\left\{(\eta - b)e^{\eta/b} - (\eta_o - b)e^{\eta_o/b}\right\} + \right.$$

$$+ C_2\left\{\left[(\eta - b)^2 + b^2\right]e^{\eta/b} - \left[(\eta_o - b)^2 + b^2\right]e^{\eta_o/b}\right\} +$$

$$+ C_3\left\{\left[\eta^3 - 3b\left[(\eta - b)^2 + b^2\right]\right]e^{\eta/b} - \left[\eta_o^3 - 3b\left[(\eta_o - b)^2 + b^2\right]\right]e^{\eta_o/b}\right\}$$

$$\left. + \cdots\right] \qquad \text{Eqn. 3.5-6}$$

where $b = RT/Z\mathcal{F}$.

It should be noticed that the coefficients of the $C-\eta$ relation (Eqn. 3.5-1) are separated uniquely in Eqn. 3.5-6 providing the form

$$t = f_0(C_0) + f_1(C_1) + f_2(C_2) + \cdots \qquad \text{Eqn. 3.5-7}$$

It may readily be shown that rearrangement of Eqn. 3.5-6 for the case of constant capacitance, i. e. C_1, C_2 and higher terms in Eqn. 3.5-1 equal to zero, leads to a result previously obtained by Frumkin [4]:

$$\eta = \eta_o + \frac{b}{\alpha} \ln\left[1 - \frac{J_0 J_T \alpha}{bC} t\right] \qquad \text{Eqn. 3.5-8}$$

The more general case for potential decay given in Eqn. 3.5-6 permits an assessment to be made of the importance of curvature in the potential-time curve near t = 0 when the capacitance is variable. This problem has often been the subject of comment, particularly when interrupter methods were used extensively. The problem remains an important one, however, since the evaluation of reaction kinetics parameters requires fitting of a relation between η and $\ell n\ t$ by the method used and further discussed by Conway and co-workers[7] [8].

An estimate of the importance of a variable capacitance may be made by considering hypothetical variations of capacitance according to the following three cases:

Case (1) C = constant = 12 μF cm^{-2}

Case (2) $C(\eta) = 4.0 - 53.4\eta$ (μF cm^{-2} when η has units of volts)

Case (3) $C(\eta) = 20.0 + 53.4\eta$

For typical values of $J_T = 0.1$ A cm^{-2}, $J_o = 10^{-3}$A cm^{-2}, $T = 300^oK$, $Z = 1$, leading to the initial steady state value $\eta_o = 238$mV. The results are shown in Fig. 1, where, according to the treatment of Morley and Wetmore[6], we have drawn the potential against the log of the time elapsed after switching off (t = 0) the constant current, plus a constant value θ, equal to bC/J_T. The slope of such decay curves has been often used for the determination of b. Due to the curvature shown for Case (2) and (3), this determination is not very precise if C is a function of η. In the three cases above, the average value of the capacitance is $C_{ave} = 12\ \mu$F cm^{-2}, and, from case (1), b = 0.0258. Using values of the slope obtained from Fig. 1, the corresponding value of b will deviate from that obtained in case (1), by an amount varying between 15% (at 88% η_o) and 30% (at 15% η_o). This shows that the determination of kinetic parameters from such decay curves should be made only if the capacity can be considered as constant in the range studied. If this is not the case, Eqn. 3.5-6 allows better precision when capacitance can be approximated as a polynomial function of potential.

References

(1) L. Nanis, P. Javet, J. Electrochem. Soc. 114, 810 (1967).

(2) D. C. Grahame, Chem. Rev. 41, 441 (1967).

(3) For a review on this subject, see R. Parsons, "Modern Aspects of Electrochemistry", Volume 1, J. O'M. Bockris ed. Academic Press, N.Y. (1954).

(4) A. Frumkin, Acta Physicochim., USSR, 18, 23 (1943).

(5) A. Hickling, F. W. Salt, Trans. Faraday Soc. 36, 1226 (1940); 37, 224, 319, 333, 450 (1941); 38, 474 (1941).

(6) H. B. Morley, F. E. W. Wetmore, Can. J. of Chem. 34, 359 (1956).

(7) B. E. Conway, P. L. Bourgault, Trans. Faraday Soc. 58, 593 (1962).

(8) B. E. Conway, E. Gileadi, H. Angerstein-Kozlowska, J. Electrochem. Soc. 112, 341 (1965).

Figure Caption

Fig. 1. Decay of activation overpotential as a function of time plus a constant, for different capacitance-potential relations.

$Z=1$; $\alpha=0.5$; $T=300^{\circ}K$; $J_T=10^{-1}$ Acm^{-2}; $J_o=10^{-3}$ Acm^{-2}.

① : c = constant = $12\,\mu F\,cm^{-2}$

② : $c(\eta) = 4.0 - 53.4\,\eta$ ($\mu F\,cm^{-2}$ when η is expressed in volts)

③ : $c(\eta) = 20.0 + 53.4\,\eta$ ($\mu F\,cm^{-2}$)

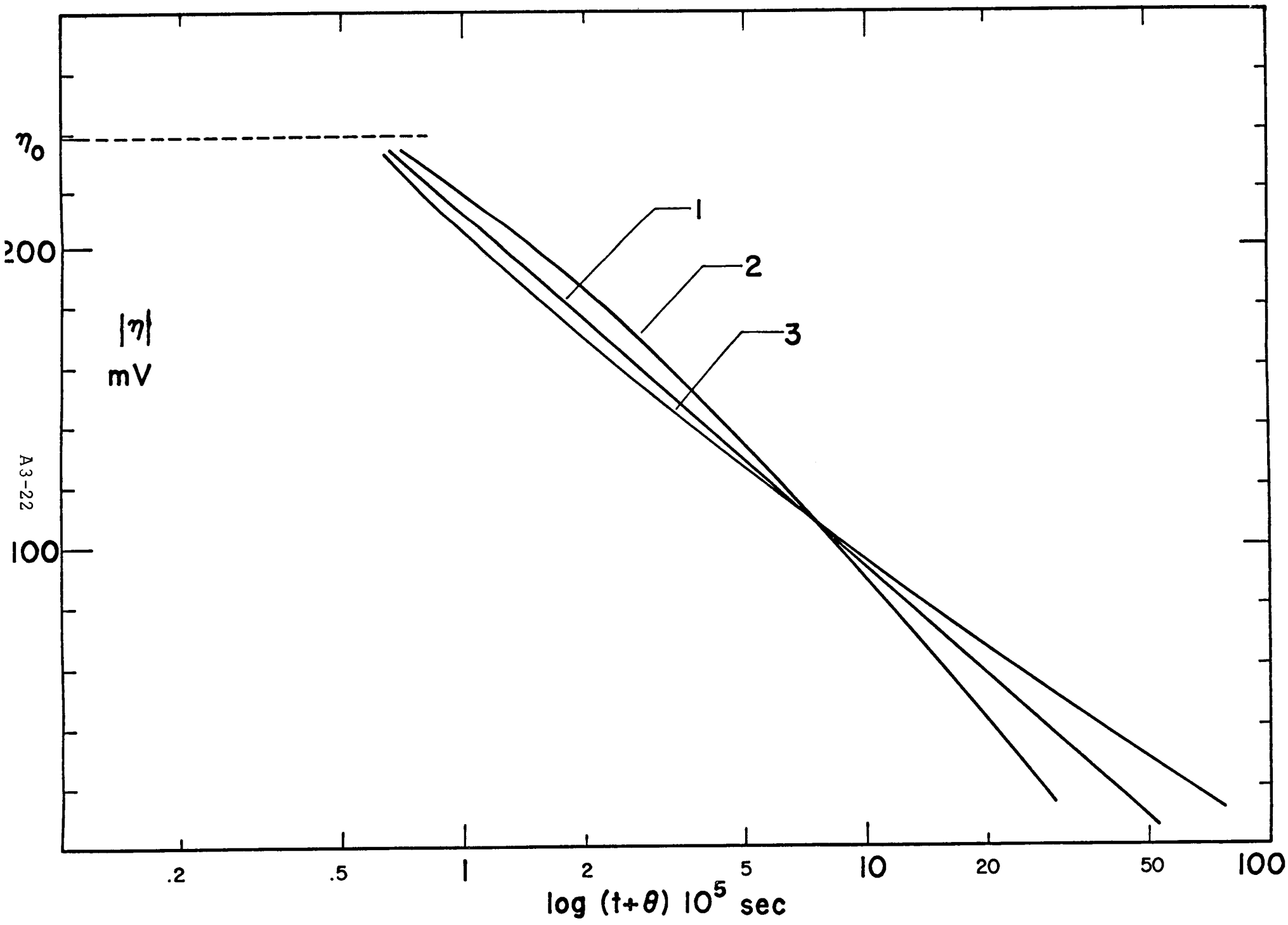
η_o
200
100
$|\eta|$
mV
1
2
3
.2
.5
1
2
5
10
20
50
100
log $(t+\theta)$ 10^5 sec